CHAPTER 17

Magnetic Resonance Imaging

Between 1978 and 1985 magnetic resonance imaging (MRI) (formerly called nuclear magnetic resonance imaging) developed into a useful modality for medical diagnosis. It provides very-high-resolution images without ionizing radiation. There is also the potential for more elaborate imaging, including phase effects, flow, and the signature of particular atomic environments.

Magnetic resonance phenomena are more complicated than x-ray attenuation or photon emission by a radioactive nucleus. Magnetic resonance imaging depends upon the behavior of atomic nuclei in a magnetic field, in particular, the orientation and motion of the nuclear magnetic moment in the magnetic field. The patient is placed in a strong static magnetic field (typically 1–4 T). This is usually provided by a hollow cylindrical (solenoidal) magnet, though some machines are being made that use other configurations so that the physician can carry out procedures on the patient while viewing the MRI image. Other coils apply spatial gradients to the magnetic field, along with radio-frequency signals that cause the magnetization changes described below. Still other coils detect the very weak radio-frequency signals resulting from these changes.

First, we must understand the property that we are measuring. Section 17.1 describes the behavior of a magnetic moment in a static magnetic field, and Sec. 17.2 shows how the nuclear spin is related to the magnetic moment. Section 17.3 introduces the concept of the magnetization vector, which is the magnetic moment per unit volume, while Sec. 17.4 develops the equations of motion for the magnetic moment. In order to describe the motion of the magnetization, it is convenient—in fact, almost mandatory—to use the rotating coordinate system described in section 17.5.

To make a measurement, the nuclear magnetic moments originally aligned with the static magnetic field are made to rotate or precess in a plane perpendicular to the static field, after which the magnetization gradually returns to its original value. This relaxation phenomenon is described in Sec. 17.6. Sections 17.7 and 17.8 describe ways in which the magnetization can be manipulated for measurement or imaging.

Imaging techniques are finally introduced in Sec. 17.9. Sections 17.10 and 17.11 describe how chemical shifts and flow can affect the image or can themselves be imaged.

17.1. MAGNETIC MOMENTS IN AN EXTERNAL MAGNETIC FIELD

Magnetic resonance imaging detects the magnetic dipoles in the nuclei of atoms in the human body. We saw in Chap. 9 that isolated magnetic monopoles have never been observed [see Eq. (9.6)], and that magnetic fields are produced by moving charges or electric currents. In some cases, such as bar magnets, the external field is the same as if there were magnetic charges occurring in pairs or *dipoles*.[1] The strength of a dipole is measured by its *magnetic dipole moment* $\boldsymbol{\mu}$. (In Chap. 9 the magnetic dipole moment was called $\mathbf{m}$ to avoid confusion with μ_0. In this chapter we use $\boldsymbol{\mu}$ to avoid confusion with the quantum number m and to be consistent with the literature in the field.) The magnetic dipole moment is analogous to the electric dipole moment of Chap. 7; however, it is produced by a movement of charge, such as charge moving in a circular path. The units of $\boldsymbol{\mu}$ are J T^{-1} or A m^2. We saw that when a magnetic dipole is placed in a magnetic field as in Fig. 17.1, it is necessary to apply an external torque $\boldsymbol{\tau}_{ext}$ to keep it in equilibrium. This torque, which is required to cancel the torque exerted by the magnetic field, vanishes if the dipole is aligned with the magnetic field. The torque exerted on the dipole by the magnetic field is

$$\boldsymbol{\tau} = \boldsymbol{\mu} \times \mathbf{B} \tag{17.1}$$

[This is Eq. (9.4)].

[1]Dipoles can be arranged so that their fields nearly cancel, giving rise to still-higher-order moments such as the quadrupole moment or the octupole moment. (See Chap. 7). A configuration for which the quadrupole moment is important is two magnets in line arranged as N-S-S-N.

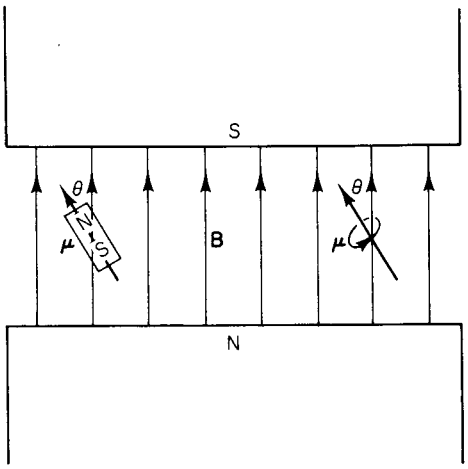

FIGURE 17.1. A dipole in a magnetic field. The dipole can be either a bar magnet or a current loop.

The potential energy of the dipole is the work that must be done by τ_{ext} to change the dipole's orientation in the magnetic field without changing any kinetic energy it might have. To increase angle θ by an amount $d\theta$ requires that work be done on the dipole–magnetic field system. This work is the increase in potential energy of the system:

$$dU = \mu B \sin\theta \, d\theta. \tag{17.2}$$

This can be integrated to give the change in potential energy when the angle changes from θ_1 to θ_2:

$$U(\theta_2) - U(\theta_1) = -\mu B(\cos\theta_2 - \cos\theta_1).$$

If the energy is considered to be zero when the dipole is at right angles to the z axis, then the potential energy is

$$U(\theta) = -\mu B \cos\theta = -\boldsymbol{\mu}\cdot\mathbf{B}. \tag{17.3}$$

In many cases the moving charges that give rise to the magnetic moment of an object possess angular momentum. Often the magnetic moment is parallel to and proportional to the angular momentum: $\boldsymbol{\mu} = \gamma\mathbf{L}$. The proportionality factor is called the *gyromagnetic ratio* (sometimes called the magnetogyric ratio). When such an object is placed in a uniform magnetic field, the resulting motion can be quite complicated. The torque on the object is $\boldsymbol{\tau} = \boldsymbol{\mu}\times\mathbf{B} = \gamma\mathbf{L}\times\mathbf{B}$. It is not difficult to show (Problem 17.1) that the torque is the rate of change of the angular momentum, $\boldsymbol{\tau} = d\mathbf{L}/dt$. Therefore the equation of motion is

$$\gamma(\mathbf{L}\times\mathbf{B}) = \frac{d\mathbf{L}}{dt} \tag{17.4a}$$

or

$$\gamma(\boldsymbol{\mu}\times\mathbf{B}) = \frac{d\boldsymbol{\mu}}{dt}. \tag{17.4b}$$

Solutions to these equations are discussed in Sec. 17.4.

17.2. THE SOURCE OF THE MAGNETIC MOMENT

Atomic electrons and the protons and neutrons in the atomic nucleus can possess both angular momentum and a magnetic moment. The magnetic moment of a particle is related to its angular momentum. We can derive this relationship for a charged particle moving in a circular orbit. We saw in Chap. 9 that the magnitude of the magnetic moment of a current loop is the product of the current i and the area of the loop S:

$$|\boldsymbol{\mu}| = \mu = iS. \tag{17.5}$$

The direction of the vector is perpendicular to the plane of the loop. Its direction is defined by a right-hand rule: curl the fingers of your right hand in the direction of current flow and your thumb will point in the direction of $\boldsymbol{\mu}$ (see the right-hand part of Fig. 17.1). This is the same right-hand rule that relates the circular motion of a particle to the direction of its angular momentum.

Suppose that a particle of charge q and mass m moves in a circular orbit as in Fig. 17.2. The speed is v and the magnitude of the angular momentum is $L = mvr$. The effective current is the charge q multiplied by the number of times it goes past a given point on the circumference of the orbit in one second:

$$i = \frac{qv}{2\pi r}.$$

The magnetic moment has magnitude

$$\mu = iS = i\pi r^2 = \frac{qvr}{2}.$$

Since the angular momentum is $L = mvr$ and $\boldsymbol{\mu}$ and $\mathbf{L}$ are both perpendicular to the plane of the orbit, we can write

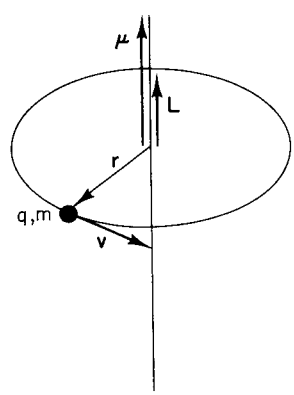

FIGURE 17.2. A particle of charge q and mass m travels in a circular orbit. It has a magnetic moment $\boldsymbol{\mu}$ and angular momentum $\mathbf{L}$. If the charge is positive, $\boldsymbol{\mu}$ and $\mathbf{L}$ are parallel; if it is negative they are in opposite directions.

$$\boldsymbol{\mu}=\left(\frac{q}{2m}\right)\mathbf{L}=\gamma\mathbf{L}. \tag{17.6}$$

The quantity $\gamma=q/2m$ is the gyromagnetic ratio for this system. The units of γ are $T^{-1}\ s^{-1}$ (see Problem 17.2). The magnetic moment and the orbital angular momentum are parallel for a positive charge and antiparallel for a negative charge.

An electron or a proton also has an intrinsic magnetic moment quite separate from its orbital motion. It is associated with and proportional to the intrinsic or "spin" angular momentum **S** of the particle. We write

$$\boldsymbol{\mu}=\gamma\mathbf{S}. \tag{17.7}$$

The value of γ for a spin is *not* equal to $q/2m$.

Two kinds of spin measurements have biological importance. One is associated with electron magnetic moments and the other with the magnetic moments of nuclei. Most neutral atoms in their ground state have no magnetic moment due to the electrons. Exceptions are the transition elements that exhibit paramagnetism. Free radicals, which are often of biological interest, have an unpaired electron and therefore have a magnetic moment. In most cases this magnetic moment is due almost entirely to the spin of the unpaired electron.

Magnetic resonance imaging is based on the magnetic moments of atomic nuclei in the patient. The total angular momentum and magnetic moment of an atomic nucleus are due to the spins of the protons and neutrons, as well as any orbital angular momentum they have inside the nucleus. Table 17.1 lists the spin and gyromagnetic ratio of the electron and some nuclei of biological interest.

If the nuclear angular momentum is **I** with quantum number I, the possible values of the z component of **I** are $I\hbar,(I-1)\hbar,\ldots,-I\hbar$. For $I=\frac{1}{2}$, the values are $\hbar/2$ and $\hbar/2$, while for $I=\frac{3}{2}$ they are $3\hbar/2$, $\hbar/2$, $-\hbar/2$ and $-3\hbar/2$. The direction of the external magnetic field defines the z axis, and the energy of a spin is given by $-\boldsymbol{\mu}\cdot\mathbf{B}=-\gamma I\cdot\mathbf{B}=-\gamma m\hbar B$. The difference between adjacent energy levels is $\gamma B\hbar$, and the angular frequency of a photon corresponding to that difference is $\omega_{\text{photon}}=\gamma B$.

TABLE 17.1. *Values of the spin and gyromagnetic ratio for a free electron and various nuclei of interest.*

Particle	Spin	$\gamma=\omega_{\text{Larmor}}/B$ ($s^{-1}\ T^{-1}$)	ν/B (MHz T^{-1})
Electron	$\frac{1}{2}$	1.7608×10^{11}	2.8025×10^{4}
Proton	$\frac{1}{2}$	2.6753×10^{8}	42.5781
Neutron	$\frac{1}{2}$	1.8326×10^{8}	29.1667
^{23}Na	$\frac{3}{2}$	0.7076×10^{8}	11.2618
^{31}P	$\frac{1}{2}$	1.0829×10^{8}	17.2349

17.3. THE MAGNETIZATION

The MRI image depends on the *magnetization* of the tissue. The magnetization of a sample, **M**, is the average magnetic moment per unit volume. In the absence of an external magnetic field to align the nuclear spins, the magnetization is zero. As an external static magnetic field is applied, the spins tend to align in spite of their thermal motion, and the magnetization increases, proportional at first to the external field. If the external field is strong enough, all of the nuclear magnetic moments are aligned, and the magnetization reaches its saturation value.

We can calculate the magnetization. Consider a collection of spins of a single nuclear species in an external magnetic field. This might be the hydrogen nuclei (protons) in a sample. The spins do not interact with each other but are in thermal equilibrium with the surroundings, which are at temperature T. We do not consider the mechanism by which they reach thermal equilibrium. Since the magnetization is the average magnetic moment per unit volume, it is the number of spins per unit volume, N, times the average magnetic moment of each spin: $\mathbf{M}=N\langle\boldsymbol{\mu}\rangle$.

To obtain the average value of the z component of the magnetic moment, we must consider each possible value of quantum number m. We multiply the value of μ_z corresponding to each value of m by the probability that m has that value. Since the spins are in thermal equilibrium with the surroundings, the probability is proportional to the Boltzmann factor of Chap. 3, $\exp(-U/k_BT)=\exp(\gamma m\hbar B/k_BT)$. The denominator in Eq. (17.8) normalizes the probability:

$$\langle\mu_z\rangle=\frac{\gamma\hbar\sum_{m=-I}^{I}m\ \exp(\gamma m\hbar B/k_BT)}{\sum_{m=-I}^{I}\exp(\gamma m\hbar B/k_BT)}. \tag{17.8}$$

At room temperature $\gamma I\hbar B/k_BT\ll1$ (see Problem 17.4), and it is possible to make the approximation $e^x\approx1+x$. The sum in the numerator then has two terms:

$$\sum_m m+\frac{\gamma\hbar B}{k_BT}\sum_m m^2.$$

The first sum vanishes. The second is $I(I+1)(2I+1)/3$. The denominator is

$$\sum_m 1+\frac{\gamma\hbar B}{k_BT}\sum_m m.$$

The first term is $2I+1$; the second vanishes. Therefore we obtain

$$\langle\mu_z\rangle=\frac{\gamma^2\hbar^2I(I+1)}{3k_BT}\,B. \tag{17.9}$$

The z component of **M** is

$$M_z=N\langle\mu_z\rangle=\frac{N\gamma^2\hbar^2I(I+1)}{3k_BT}\,B, \tag{17.10}$$

which is proportional to the applied field.

17.4. BEHAVIOR OF THE MAGNETIZATION VECTOR

A remarkable result of quantum mechanics is that the average or expectation value of a spin obeys the classical Equation (17.4b):

$$\frac{d\langle\boldsymbol{\mu}\rangle}{dt}=\gamma(\langle\boldsymbol{\mu}\rangle\times\mathbf{B}) \tag{17.11}$$

whether or not **B** is time dependent [Slichter (1978), p. 20]. Multiplying by the number of spins per unit volume we obtain

$$\frac{d\mathbf{M}}{dt}=\gamma(\mathbf{M}\times\mathbf{B}) \tag{17.12}$$

This equation can lead to many different behaviors of **M**, some of which are quite complicated.

The simplest motion occurs if **M** is parallel to **B**, in which case **M** does not change because there is no torque. Another relatively simple motion, called *precession*, is shown in Figure 17.3. With the proper initial conditions **M** (and $\langle\boldsymbol{\mu}\rangle$) precess about the direction of **B**. That is, they both rotate about the direction of **B** with a constant angular velocity and at a fixed angle θ with the direction of **B**. Since $\mathbf{M}\times\mathbf{B}$ is always at right angles to **M**, $d\mathbf{M}/dt$ is at right angles to **M**, and the angular momentum does not change magnitude. The analytic solution can be investigated by writing Eq. (17.12) in Cartesian coordinates when **B** is along the z axis:

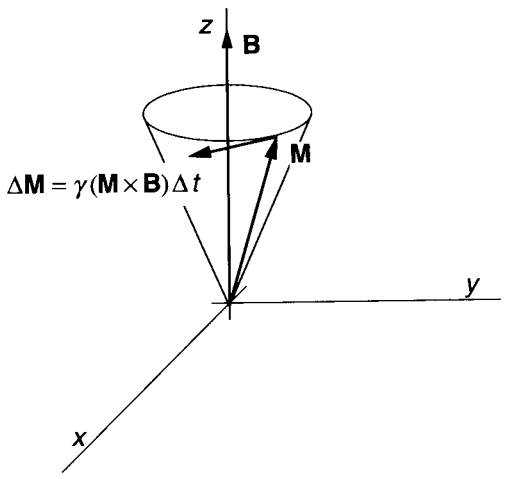

FIGURE 17.3. The system with initial magnetization **M** has been given just enough additional angular momentum to precess about the direction of the static magnetic field **B**. The rate of change of **M** is perpendicular to both **M** and **B**. For short time intervals, $\Delta\mathbf{M}=\gamma(\mathbf{M}\times\mathbf{B})\Delta t$.

$$\frac{dM_x}{dt}=\gamma M_y B_z,$$

$$\frac{dM_y}{dt}=-\gamma M_x B_z, \tag{17.13}$$

$$\frac{dM_z}{dt}=0.$$

One possible solution to these equations is

$$M_z=M_\parallel=\text{const},$$

$$M_x=M_\perp\cos(-\omega t), \tag{17.14}$$

$$M_y=M_\perp\sin(-\omega t).$$

You can verify that these are a solution for arbitrary values of $M_\parallel$ and $M_\perp$ as long as $\omega=\omega_0=\gamma B_z$. This is called the *Larmor precession frequency*. The minus sign means that for positive γ the rotation is clockwise in the xy plane. The classical Larmor frequency is equal to the frequency of photons corresponding to the energy difference given by successive values of $\boldsymbol{\mu}\cdot\mathbf{B}$. For this solution the initial values of **M** at $t=0$ are $M_x(0)=M\perp$, $M_y(0)=0$, and $M_z(0)=M_\parallel$.

We need to modify the equation of motion, Eq. (17.12), to include changes in **M** that occur because of effects other than the magnetic field. Suppose that **M** has somehow been changed so that it no longer points along the z axis with the equilibrium value given by Eq. (17.10). Thermal agitation will change the populations of the levels so that M_z returns to the equilibrium value, which we call M_0. We *postulate* that the rate of exchange of energy with the reservoir is proportional to how far the value of M_z is from equilibrium:

$$\frac{dM_z}{dt}=\frac{1}{T_1}(M_0-M_z).$$

The quantity T_1, which is the inverse of the proportionality constant, is called the *longitudinal relaxation time* or *spin–lattice relaxation time.*

We also *postulate* an exponential disappearance of the x and y components of **M**. (This assumption is often not a good one. For example, the decay of M_x and M_y in ice is more nearly Gaussian than exponential.) The equations are

$$\frac{dM_x}{dt}=-\frac{M_x}{T_2},\quad \frac{dM_y}{dt}=-\frac{M_y}{T_2}.$$

The *transverse relaxation time* T_2 (sometimes called the spin–spin relaxation time) is always shorter than T_1. A change of M_z requires an exchange of energy with the reservoir. This is not necessary for changes confined to the xy plane, since the potential energy ($\boldsymbol{\mu}\cdot\mathbf{B}$) does not change in that case. M_x and M_y can change as M_z changes, but they can also change by other mechanisms, such as when individual spins precess at slightly different frequencies, a process known as *dephasing*. The angular velocity of

precession of $\boldsymbol{\mu}$ can be slightly different for different nuclear spins because of local variations in the static magnetic field; the angular velocity can also fluctuate as the field fluctuates with time. These variations and fluctuations are caused by neighboring atomic or nuclear magnetic moments or by inhomogeneities in the external magnetic field **B**. Figure 17.4 shows how dephasing occurs if several magnetic moments precess at different rates.

Combining these approximate equations for relaxation in the absence of an applied magnetic field with Eq. (17.12) for the effect of a magnetic field gives the *Bloch equations*:

$$\frac{dM_z}{dt}=\frac{1}{T_1}(M_0-M_z)+\gamma(\mathbf{M}\times\mathbf{B})_z,$$

$$\frac{dM_x}{dt}=-\frac{M_x}{T_2}+\gamma(\mathbf{M}\times\mathbf{B})_x, \qquad (17.15)$$

$$\frac{dM_y}{dt}=-\frac{M_y}{T_2}+\gamma(\mathbf{M}\times\mathbf{B})_y.$$

While these equations are not rigorous and there is no reason for the relaxation to be strictly exponential, they have proven to be quite useful in explaining many facets of nuclear spin magnetic resonance.

One can demonstrate by direct substitution the following solution to Eqs. (17.15) for a static magnetic field **B** along the z axis:

$$M_x=M_0e^{-t/T_2}\cos(-\omega_0t),$$

$$M_y=M_0e^{-t/T_2}\sin(-\omega_0t), \qquad (17.16)$$

$$M_z=M_0(1-e^{-t/T_1}),$$

where $\omega_0=\gamma B$. This solution corresponds to what happens if **M** is somehow made to precess in the xy plane. (We will see how to accomplish this in Sec. 17.5.) The magnetization in the xy plane is initially M_0, and the amplitude decays exponentially with time constant T_2. The initial value of M_z is zero, and it "decays" back to M_0 with time constant T_1. A perspective plot of the trajectory of the tip of vector **M** is shown in Fig. 17.5.

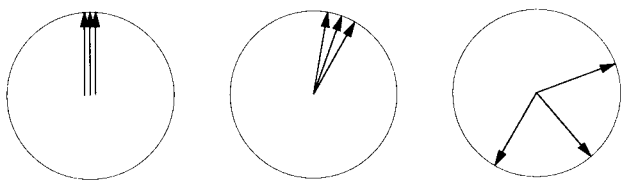

FIGURE 17.4. If two spins precess in the xy plane at slightly different rates, the total spin amplitude decreases due to dephasing.

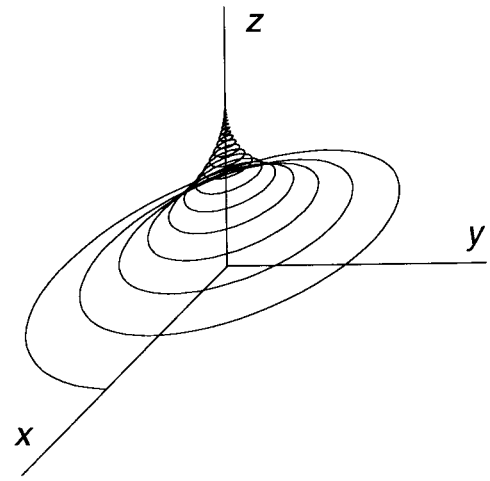

FIGURE 17.5. The locus of the tip of the magnetization **M** when it relaxes according to Eqs. (17.16).

17.5. A ROTATING COORDINATE SYSTEM

It is *much* easier to describe the motion of **M** in a coordinate system which is rotating at the Larmor frequency. Figure 17.6 shows a vector **M** and two coordinate systems, xy and $x'y'$. Components of **M** along each axis are also shown. By considering the components we see that

$$M_x=M_{x'}\cos\theta-M_{y'}\sin\theta,$$

$$M_y=M_{x'}\sin\theta+M_{y'}\cos\theta.$$

For a three-dimensional coordinate system rotating clockwise around the z axis, $\theta=-\omega t$, the z-component of **M** is unchanged, and the transformation equations are

$$M_x=M_{x'}\cos(-\omega t)-M_{y'}\sin(-\omega t),$$

$$M_y=M_{x'}\sin(-\omega t)+M_{y'}\cos(-\omega t), \qquad (17.17)$$

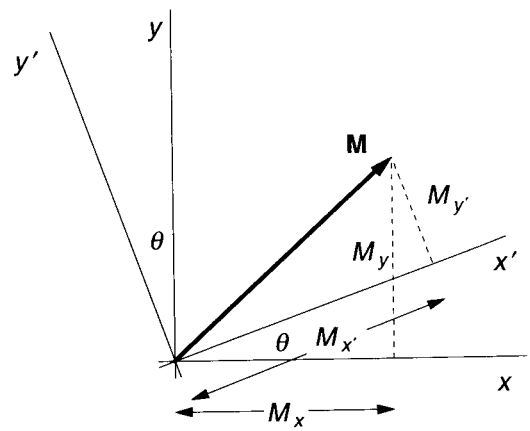

FIGURE 17.6. The vector **M** can be represented by components along x and y or along x' and y'.

$$M_z = M_{z'}.$$

The time derivative of $\mathbf{M}$ is obtained by differentiating each component and remembering that $\mathbf{M}'$ can also depend on t:

$$\frac{dM_x}{dt} = \frac{dM_{x'}}{dt}\cos(-\omega t) - \frac{dM_{y'}}{dt}\sin(-\omega t) + \omega M_{x'}\sin(-\omega t) + \omega M_{y'}\cos(-\omega t),$$

$$\frac{dM_y}{dt} = \frac{dM_{x'}}{dt}\sin(-\omega t) + \frac{dM_{y'}}{dt}\cos(-\omega t) - \omega M_{x'}\cos(-\omega t) + \omega M_{y'}\sin(-\omega t), \tag{17.18}$$

$$\frac{dM_z}{dt} = \frac{dM_{z'}}{dt}.$$

We can use these expressions to write the equations of motion in the rotating frame. First consider a system without relaxation effects and with a static field B_z along the z axis. We will show that the components of $\mathbf{M}$ in a system rotating at the Larmor frequency are constant. The equations of motion are given in Eqs. (17.13). In terms of variables in the rotating frame, the equation for dM_x/dt becomes

$$\frac{dM_{x'}}{dt}\cos(-\omega t) - \frac{dM_{y'}}{dt}\sin(-\omega t) + \omega M_{x'}\sin(-\omega t) + \omega M_{y'}\cos(-\omega t) = \gamma[M_{x'}\sin(-\omega t) + M_{y'}\cos(-\omega t)]B_z.$$

If the frame rotates at the Larmor frequency $\omega_0 = \gamma B_z$, the third and fourth terms on the left are equal to the right-hand side. The equation becomes

$$\frac{dM_{x'}}{dt}\cos(-\omega_0 t) - \frac{dM_{y'}}{dt}\sin(-\omega_0 t) = 0.$$

Under the same circumstances, the equation for dM_y/dt gives

$$\frac{dM_{x'}}{dt}\sin(-\omega_0 t) + \frac{dM_{y'}}{dt}\cos(-\omega_0 t) = 0.$$

Solving these simultaneously shows that $dM_{x'}/dt = 0$ and $dM_{y'}/dt = 0$. Therefore in the rotating system $M_{x'}$ and $M_{y'}$ are constant. Equation (17.13) showed that M_z is constant, so the components of $\mathbf{M}$ are constant in the frame rotating at the Larmor frequency. Using Eqs. (17.17) to transform back to the laboratory system gives the solution Eq. (17.14).[2]

The next problem we consider in the rotating coordinate system is the addition of an oscillating magnetic field $B_1\cos(\omega t)$ along the x axis, fixed in the laboratory system. We will show that if the applied field is at the Larmor frequency, the equations of motion in the rotating system, Eqs. (17.24), are quite simple but very important. They are given as Eqs. (17.24) below.

They are derived as follows. From the x component of Eq. (17.12),

$$\frac{dM_x}{dt} = \gamma(M_y B_z - M_z B_y),$$

we obtain (remembering that the $x'y'$ system is rotating at the Larmor frequency ω_0)

$$\frac{dM_{x'}}{dt}\cos(-\omega_0 t) - \frac{dM_{y'}}{dt}\sin(-\omega_0 t) + \omega_0 M_{x'}\sin(-\omega_0 t) + \omega_0 M_{y'}\cos(-\omega_0 t) = \gamma B_z[M_{x'}\sin(-\omega_0 t) + M_{y'}\cos(-\omega_0 t)].$$

Since $\omega_0 = \gamma B_z$, the last two terms on the left cancel the terms on the right, leaving

$$\frac{dM_{x'}}{dt}\cos(-\omega_0 t) - \frac{dM_{y'}}{dt}\sin(-\omega_0 t) = 0. \tag{17.19}$$

Similarly, the y-component of Eq. (17.12),

$$\frac{dM_y}{dt} = \gamma(M_z B_x - M_x B_z),$$

transforms to (remembering that $M_z = M_{z'}$)

$$\frac{dM_{x'}}{dt}\sin(-\omega_0 t) + \frac{dM_{y'}}{dt}\cos(-\omega_0 t) - \omega_0 M_{x'}\cos(-\omega_0 t) + \omega_0 M_{y'}\sin(-\omega_0 t) = \gamma M_{z'} B_1\cos(\omega t) - \gamma B_z[M_{x'}\cos(-\omega_0 t) - M_{y'}\sin(-\omega_0 t)],$$

which reduces to

$$\frac{dM_{x'}}{dt}\sin(-\omega_0 t) + \frac{dM_{y'}}{dt}\cos(-\omega_0 t) = \gamma B_1 M_{z'}\cos(\omega t). \tag{17.20}$$

The z-component of Eq. (17.12) is

$$\frac{dM_{z'}}{dt} = \gamma(M_x B_y - M_y B_x), \tag{17.21}$$

which transforms to

$$\frac{dM_{z'}}{dt} = -\gamma B_1 M_{x'}\cos(\omega t)\sin(-\omega_0 t) - \gamma B_1 M_{y'}\cos(\omega t)\cos(-\omega_0 t).$$

It is possible to eliminate $M_{x'}$ from Eqs. (17.19) and (17.20) by multiplying Eq. (17.19) by $-\sin(-\omega_0 t)$, multiplying Eq. (17.20) by $\cos(-\omega_0 t)$, and adding. The result is

$$\frac{dM_{y'}}{dt} = \gamma B_1 M_{z'}\cos(\omega_1 t)\cos(-\omega_0 t). \tag{17.22}$$

[2]For those familiar with vector analysis, the general relationship between the time derivative of any vector $\mathbf{M}$ in the laboratory system and a system rotating with angular velocity $\boldsymbol{\Omega}$ is

$$\left(\frac{d\mathbf{M}}{dt}\right)_{\text{laboratory}} = \left(\frac{\partial \mathbf{M}}{\partial t}\right)_{\text{rotating}} + \boldsymbol{\Omega}\times\mathbf{M}.$$

This can be applied to the magnetization combined with Eq. 17.21 to give

$$\left(\frac{\partial \mathbf{M}}{\partial t}\right)_{\text{rot}} = \gamma(\mathbf{M}\times\mathbf{B}) - \boldsymbol{\Omega}\times\mathbf{M} = \gamma\mathbf{M}\times\left(\mathbf{B} + \frac{\boldsymbol{\Omega}}{\gamma}\right),$$

which vanishes if $\gamma\mathbf{B} = -\boldsymbol{\Omega}$.

A similar technique can be used to eliminate $M_{y'}$ from these two equations, giving

$$\frac{dM_{x'}}{dt}=\gamma B_1 M_{z'}\sin(\omega t)\cos(-\omega_0 t). \tag{17.23}$$

Equations (17.21)–(17.23) are the equations of motion for the components of **M** in the rotating system. If $\omega\neq\omega_0$, the motion is complicated but averaged over many Larmor periods the right-hand side of each equation is zero. If the applied field oscillates at the Larmor frequency, $\omega=\omega_0$, then the $\cos^2(\omega_0 t)$ factors average to $\frac{1}{2}$ while factors like $\sin(\omega_0 t)\cos(-\omega_0 t)$ average to zero.

The averaged equations are our very important result:

$$\frac{dM_{x'}}{dt}=0 \tag{17.24a}$$

$$\frac{dM_{y'}}{dt}=\frac{\gamma B_1}{2}M_{z'}, \tag{17.24b}$$

$$\frac{dM_{z'}}{dt}=-\frac{\gamma B_1}{2}M_{y'}. \tag{17.24c}$$

The first equation says that if $M_{x'}$ is initially zero, it remains zero. Let us define a new angular frequency

$$\omega_1=\frac{\gamma B_1}{2}. \tag{17.25}$$

It is the frequency of nutation or rotation caused by B_1 oscillating at the Larmor frequency. It is much lower than the Larmor frequency because $B_1\ll B_z$. In terms of it, Eqs. (17.24b) and (17.24c) become

$$\frac{dM_{z'}}{dt}=-\omega_1 M_{y'},\quad \frac{dM_{y'}}{dt}=\omega_1 M_{z'}.$$

These are a pair of coupled linear differential equations with constant coefficients. Differentiating one and substituting it in the other gives

$$\frac{d^2M_{z'}}{dt^2}=-\omega_1\frac{dM_{y'}}{dt}=-\omega_1^2 M_{z'}, \tag{17.26}$$

which has a solution (a and b are constants of integration)

$$M_{z'}=a\sin(\omega_1 t)+b\cos(\omega_1 t). \tag{17.27}$$

From Eq. (17.24c) we get

$$M_{y'}=-\frac{1}{\omega_1}\frac{dM_{z'}}{dt}=-a\cos(\omega_1 t)+b\sin(\omega_1 t). \tag{17.28}$$

The values of a and b are determined from the initial conditions. For example, if **M** is initially along the z axis, $a=0$ and $b=M_0$. Then

$$M_{x'}=0,$$

$$M_{y'}=M_0\sin(\omega_1 t), \tag{17.29}$$

$$M_{z'}=M_0\cos(\omega_1 t).$$

This kind of motion—precession about the z axis combined with a change of the projection of **M** on z—is called *nutation*. From Eqs. (17.29) it is easy to see that turning B_1 on for a quarter of a period of ω_1 (a 90° pulse or $\pi/2$ pulse, $t=T/4=\pi/2\omega_1$ nutates **M** into the $x'y'$ plane, while a 180° or π pulse nutates **M** to point along the $-z$ axis. **M** nutates about the rotating x' axis. Shifting the phase of B_1 changes the axis in the $x'y'$ plane about which **M** nutates. It may seem strange that an oscillating magnetic field pointing along an axis fixed in the laboratory frame causes rotation about an axis in the rotating frame. The reason is that B_1 is also oscillating at the Larmor frequency, so that its amplitude changes in just the right way to cause this behavior of **M**. Figures 17.7 and 17.8 show this nutation in both the rotating frame and the laboratory frame for a $\pi/2$ pulse and a π pulse.

Figure 17.7(c) emphasizes the difference between nutation and relaxation by plotting M_z vs the projection of **M** in the $x'y'$ plane. For nutation the components of **M** are given by Eqs. (17.29), the magnitude of **M** is unchanged, and the locus is a circle. For relaxation the components are given by Eqs. (17.16).

Another interesting solution is one for which the initial value of **M** is

$$M_{x'}(0)=M_0\cos\alpha,$$

$$M_{y'}(0)=M_0\sin\alpha,$$

$$M_{z'}(0)=0.$$

This corresponds to an **M** that has already been nutated into the $x'y'$ plane. Substituting these values in Eqs. (17.27) and (17.28) shows that $b=0$ and $a=-M_0\sin\alpha$. Then the solution is

$$M_{x'}(t)=M_0\cos\alpha,$$

$$M_{y'}(t)=M_0\sin\alpha\cos(\omega_1 t),$$

$$M_{z'}(t)=-M_0\sin\alpha\sin(\omega_1 t) \tag{17.30}$$

This solution is plotted in Fig. 17.9 in both the rotating frame and the laboratory frame for the case of a π pulse (a pulse of duration π/ω_1). The effect is to nutate **M** about the x' axis in the rotating coordinate system. We will see later that this is a very useful pulse.

17.6. RELAXATION TIMES

Since longitudinal relaxation changes the value of M_z and hence $\boldsymbol{\mu}\cdot\mathbf{B}$, it is associated with a change of energy of the nucleus. The principal force that can do work on the nuclear spin and change its energy arises from the fact that the nucleus is in a fluctuating magnetic field due to neighboring nuclei and the electrons in paramagnetic atoms.

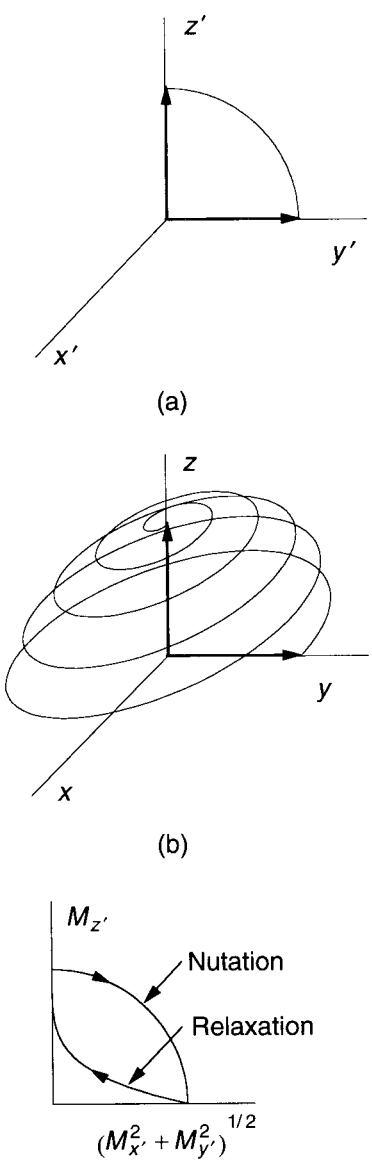

FIGURE 17.7. The locus of the tip of the magnetization **M** when an oscillating magnetic field B_1 is applied for a time t such that $\omega t = \pi/2$. This is often called a "$\pi/2$ pulse." (a) The rotating frame. (b) The laboratory frame. (c) Plots of M_z vs $(M_x^2 + M_y^2)^{1/2}$ showing the difference between nutation and relaxation.

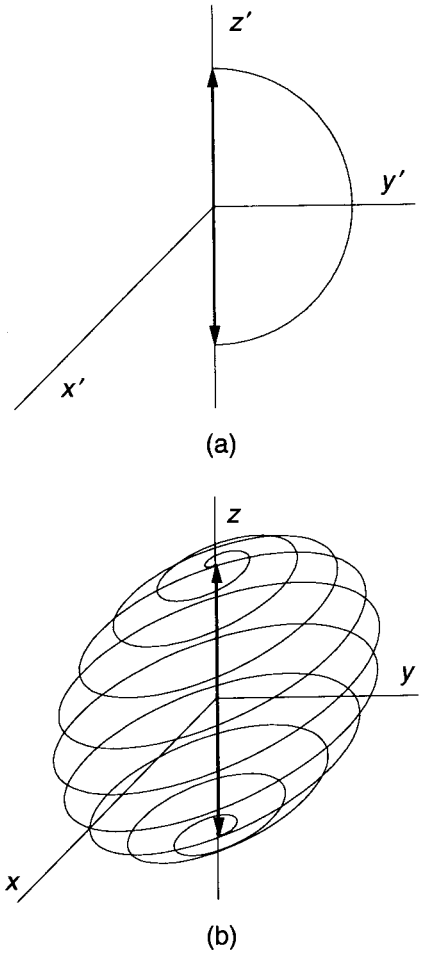

FIGURE 17.8. A pulse of B_1 applied twice as long rotates **M** to point along the $-z$ axis. (a) The rotating frame. (b) The laboratory frame.

One way to analyze the effect of this magnetic field is to say that the change of spin energy ΔE is accompanied by the emission or absorption of a photon of frequency $\omega_{\text{photon}} = \Delta E/\hbar$, or $\omega_{\text{photon}} = \omega_0$. An increase of spin energy requires the absorption of a photon at the Larmor frequency. This will have a high probability if the fluctuating magnetic field has a large Fourier component at the Larmor frequency. A decrease of spin energy is accompanied by the emission of a photon. This can happen spontaneously in a vacuum (*spontaneous emission*), or it can be stimulated by the presence of other photons at the Larmor frequency (*stimulated emission*). These relative probabilities can be calculated using quantum mechanics. Stimulated emission or absorption is much more probable than is spontaneous emission. If the random magnetic field at the nucleus changes rapidly enough due to molecular motion, it will have Fourier components at the Larmor frequency that can induce transitions that cause M_z to change. To get an idea of the strength of the field involved, consider the field at one hydrogen nucleus in a water molecule due to the other hydrogen nucleus. The field due to a magnetic dipole is given by

$$B_r = \frac{\mu_0}{4\pi}\frac{2\mu}{r^3}\cos\theta,$$

$$B_\theta = \frac{\mu_0}{4\pi}\frac{\mu}{r^3}\sin\theta,$$

$$B_\phi = 0, \tag{17.31}$$

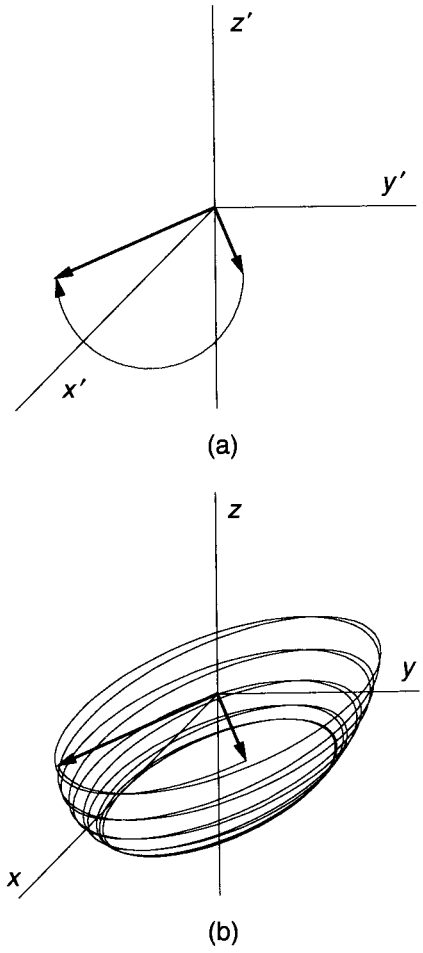

FIGURE 17.9. A magnetic field B_1 pointing along the laboratory x axis and oscillating at the Larmor frequency causes nutation of **M** around the rotating x' axis. In this case **M** was initially in the xy plane. The motion shown here is plotted from Eqs. (17.29) in (a) the rotating and (b) the laboratory frames.

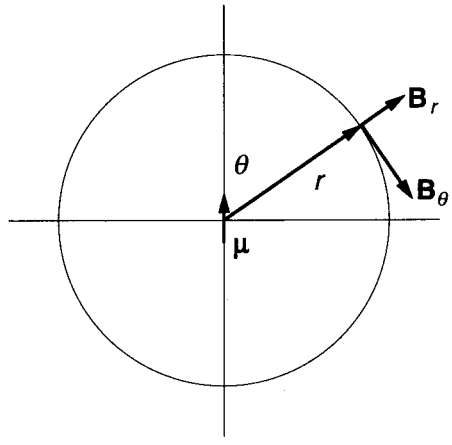

FIGURE 17.10. The magnetic field components of a dipole in spherical coordinates point in the directions shown.

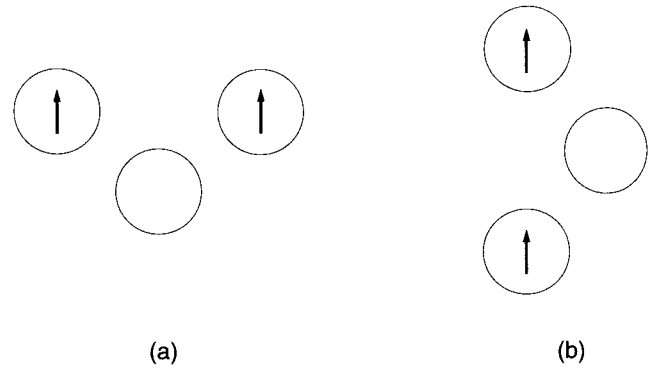

FIGURE 17.11. The z components of the magnetic moments of two protons in a water molecule are shown for two different molecular orientations, *a* and *b*. When the water molecule is fixed in space, as in ice, the magnetic field that one proton produces in the neighborhood of the other is static. When the water molecule tumbles, as in a liquid or gas, the field that one proton produces at the other changes with time.

where angle θ is defined in Fig. 17.10. (The factor $\mu_0/4\pi \equiv 10^{-7}\,\mathrm{T\,m\,A^{-1}}$ is required in SI units.) The magnetic field at one hydrogen nucleus in a water molecule due to the other hydrogen nucleus is about $(3-4)\times 10^{-4}$ T (see Problem 17.13). Consider the water molecule shown in Fig. 17.11. We refer to each hydrogen nucleus as a proton. The z components of the proton magnetic moments are shown. If the water molecule is oriented as in Fig. 17.11(a), the field at one proton due to the other has a certain value. If the water molecule remains fixed in space, as in ice, the field is constant with time. If the molecule is tumbling as in liquid water, the orientation changes as in Fig. 17.11(b), and the field changes with time.

When the molecules are moving randomly, the fluctuating magnetic field components are best described by their autocorrelation functions. The simplest assumption one can make[3] is that the autocorrelation function of each magnetic field component is exponential and that each field component has the same correlation time τ_C:

$$\phi_{11}(\tau) \propto \exp(-|\tau|/\tau_c). \tag{17.32}$$

The Fourier transform of the autocorrelation function gives the power at different frequencies. It has only cosine terms because the autocorrelation is even. Comparison with the Fourier transform pair of Eq. (11.100) shows that the power at frequency ω is proportional to $\tau_C/(1+\omega^2\tau_C^2)$. With the assumption that the transition rate, which is $1/T_1$, is proportional to the power at the Larmor frequency, we have [see also Slichter (1978), p. 167, or Dixon *et al.* (1985)]

[3] A more complete model recognizes that different atoms experience fluctuating fields with different correlation times and that frequency components at twice the Larmor frequency also contribute.

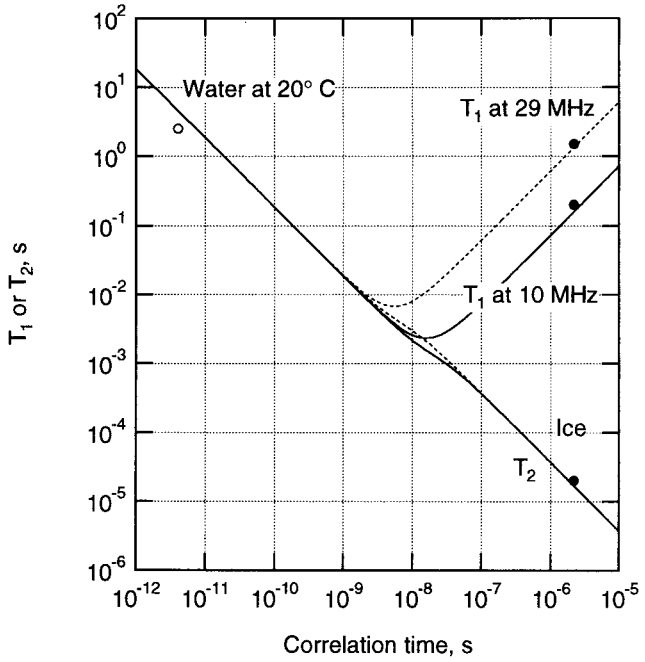

FIGURE 17.12. Plot of T_1 and T_2 vs correlation time of the fluctuating magnetic field at the nucleus. Experimental points are shown for water (open dot) and ice (solid dot).

$$\frac{1}{T_1}=\frac{C\tau_c}{1+\omega_0^2\tau_c^2}, \tag{17.33}$$

where C is the proportionality constant.

The correlation time in a solid is much longer than in a liquid. For example, in liquid water at 20 °C it is about 3.5×10^{-12} s; in ice it is about 2×10^{-6} s. Figure 17.12 shows the behavior of T_1 as a function of correlation time, plotted from Eq. (17.33) with $C=5.43\times10^{10}$ s^{-2}. For short correlation times T_1 does not depend on the Larmor frequency. At long correlation times T_1 is proportional to the Larmor frequency, as can be seen from Eq. (17.33). The minimum in T_1 occurs when $\omega_0=1/\tau_c$ in this model.

Table 17.2 shows some typical values of the relaxation times at 20 MHz. Neighboring paramagnetic atoms reduce the relaxation time by causing a fluctuating magnetic field. For example, adding 20 ppm of Fe^{3+} to water reduces T_1 to 20 ms.

Differences in relaxation time are easily detected in an image. Different tissues have different relaxation times. A contrast agent containing gadolinium is often used in magnetic resonance imaging. It is combined with many of the same pharmaceuticals used with ^{99m}Tc, and it reduces the relaxation time of nearby nuclei. The hemoglobin that carries oxygen in the blood exists in two forms: oxyhemoglobin and deoxyhemoglobin. The former is diamagnetic and the latter is paramagnetic, so the relaxation time in blood depends on the amount of oxygen in the hemoglobin. The technique that exploits this is called BOLD (blood oxygen level dependence).

TABLE 17.2. *Approximate relaxation times at 20 MHz.*

	T_1 (ms)	T_2 (ms)
Whole blood	900	200
Muscle	500	35
Fat	200	60
Water	3000	3000

It was pointed out in Sec. 17.4 that because of dephasing, T_2 is less than or equal to T_1. The same model for the fluctuating fields which led to Eq. (17.33) gives an expression for T_2:

$$\frac{1}{T_2}=\frac{C\tau_c}{2}+\frac{1}{2T_1}. \tag{17.34}$$

There is a slight frequency dependency to T_2 for values of the correlation time close to the reciprocal of the Larmor frequency.

Another effect that causes the magnetization to rapidly decrease is dephasing. Dephasing across the sample occurs because of inhomogeneities in the externally applied field. Suppose that the spread in Larmor frequency and the transverse relaxation time are related by $T_2\Delta\omega=K$. (Usually K is taken to be 2.) The spread in Larmor frequencies $\Delta\omega$ is due to a spread in magnetic field ΔB experienced by the nuclear spins in different atoms. The total variation in B is due to fluctuations caused by the magnetic field of neighbors and to variation in the applied magnetic field across the sample:

$$\Delta B_{\text{tot}}=\Delta B_{\text{internal}}+\Delta B_{\text{external}}.$$

Therefore

$$\Delta\omega_{\text{tot}}=\Delta\omega_{\text{internal}}+\Delta\omega_{\text{external}}.$$

The total spread is associated with the experimental relaxation time, $T_2^*=K/\Delta\omega_{\text{tot}}$. The "true" or "non-recoverable" relaxation time $T_2=K/\Delta\omega_{\text{internal}}$ is due to the fluctuations in the magnetic field intrinsic to the sample. Therefore

$$\frac{1}{T_2^*}=\frac{1}{T_2}+\frac{\gamma\Delta B_{\text{external}}}{K}. \tag{17.35}$$

T_2 is called the *nonrecoverable* relaxation time because various experimental techniques can be used to compensate for the external inhomogeneities, but not the atomic ones.

17.7. DETECTING THE SIGNAL

We have now seen that a sample of nuclear spins in a strong magnetic field has an induced magnetic moment, that it is possible to apply a sinusoidally varying magnetic field and nutate the magnetic moment to precess at any arbitrary

angle with respect to the static field, and that the magnetization then relaxes or returns to its original state with two characteristic time constants, the longitudinal and transverse relaxation times. We next consider how a useful signal can be obtained from these spins. This is done be measuring the weak magnetic field generated by the magnetization as it precesses in the xy plane.

Suppose that one has a sample at the origin. The motions plotted in Fig. 17.7 suggest that one way to produce a magnetization rotating in the xy plane is to have a static field along the z axis, combined with a coil in the yz plane (perpendicular to the x axis) connected to a generator of alternating current at frequency ω_0. Turning on the generator for a time $\Delta t = \pi/2\omega_1 = \pi/\gamma B_1$ rotates the magnetization into the xy plane. This is called a *90° pulse* or *π/2 pulse*. If the generator is then turned off, the same coil can be used to detect the changing magnetic flux due to the rotating magnetic moments. The resulting signal, an exponentially damped sine wave, is called the *free induction decay* (FID).

To estimate the size of the signal induced in the coil, imagine a magnetic moment $\boldsymbol{\mu} = \mathbf{M}\,\Delta V$ rotating in the xy plane as shown in Fig. 17.13. The voltage induced in a one-turn coil in the yz plane is the rate of change of the magnetic flux through the coil:

$$\Delta v = -\frac{\partial \Phi}{\partial t} = -\frac{\partial}{\partial t}\int \mathbf{B}\cdot d\mathbf{S}.$$

The magnetic field far from a magnetic dipole can be written most simply in spherical coordinates [Eqs. (17.31)]. We need the flux through the coil of radius a in the yz plane. However, Eqs. (17.31) are not valid close to the dipole. Since a fundamental property of the magnetic field is that for a closed surface $\int\int \mathbf{B}\cdot d\mathbf{S} = 0$, the flux Φ through the coil in Fig. 17.13 is the negative of the flux through the hemispherical cap in Fig. 17.14:

$$\Phi = -\int B_r 2\pi a^2 = -\frac{\mu_0}{4\pi}\frac{4\pi\mu_x}{a}\int_0^{\pi/2} \cos\theta \sin\theta\, d\theta$$

$$= -\frac{\mu_0}{4\pi}\frac{2\pi\mu_x}{a}. \tag{17.36}$$

At any instant $\boldsymbol{\mu}$ can be resolved into components along x and y. The component pointing along y contributes no net flux through the spherical cap of Fig. 17.14. Therefore, the flux for a magnetic moment $\boldsymbol{\mu} = \mathbf{M}\,\Delta V$, where $\mathbf{M}$ is given by Eqs. (17.16), is

$$\Phi = -\frac{\mu_0}{4\pi}\frac{2\pi M_0 \Delta V}{a} e^{-t/T_2}\cos(-\omega_0 t).$$

The induced voltage is $-\partial\Phi/\partial t$:

$$v = \frac{\mu_0}{4\pi}\frac{2\pi M_0 \Delta V}{a} e^{-t/T_2}\left(\frac{1}{T_2}\cos(-\omega_0 t) + \omega_0 \sin(-\omega_0 t)\right).$$

Since $1/T_2 \ll \omega_0$, this can be simplified to

$$v = \frac{\mu_0}{4\pi}\frac{\omega_0}{a} 2\pi M_0 \Delta V\, e^{-t/T_2}\sin(-\omega_0 t).$$

If the value of M_z which exists at thermal equilibrium has been nutated into the xy plane, then M_0 is given by the M_z of Eq. (17.10). For a spin-$\frac{1}{2}$ particle (and using the fact that $\omega_0 = \gamma B_0$) we obtain

$$v = -\frac{\mu_0}{4\pi}\frac{\pi N\,\Delta V\,\gamma^3\hbar^2 B_0^2}{2k_B T a} e^{-t/T_2}\cos(-\omega_0 t). \tag{17.37}$$

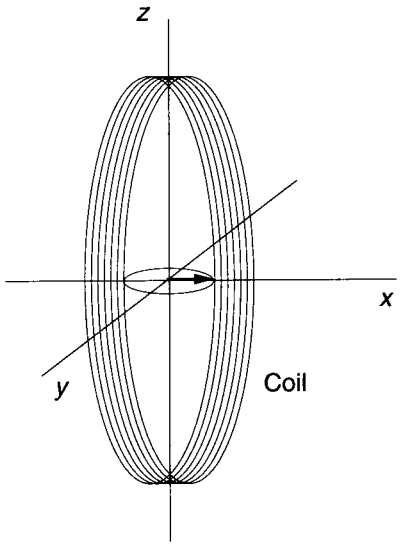

FIGURE 17.13. A magnetic moment rotating in the xy plane induces a voltage in a pickup coil in the yz plane.

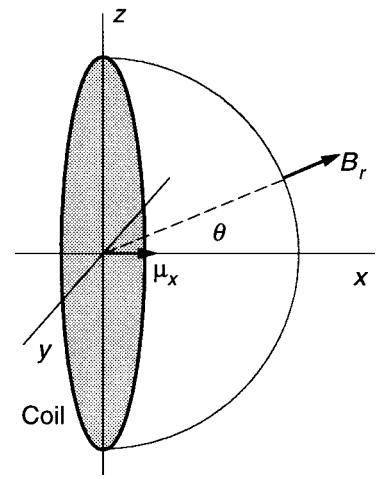

FIGURE 17.14. A dipole along the x axis generates a flux through the circle in the yz plane that is equal and opposite to that through the spherical cap.

Here $N\ \Delta V$ is the total number of nuclear spins involved, B_0 is the field along the z axis, and a is the radius of the coil that detects the free-induction-decay signal. For a volume element of fixed size, as in magnetic resonance imaging, the sensitivity is inversely proportional to the coil radius. If the sample fills the coil, as in most laboratory spectrometers, then the sensitivity is proportional to a.

17.8. SOME USEFUL PULSE SEQUENCES

Many different ways of applying radio-frequency pulses to generate B_1 have been developed by nuclear magnetic resonance spectroscopists for measuring relaxation times. There are five "classic" sequences, which also form the basis for magnetic resonance imaging.

17.8.1. Free-Induction-Decay (FID) Sequence

Free induction decay was described in Sec. 17.7. A $\pi/2$ pulse nutates **M** into the xy plane, where its precession induces a signal in a pickup coil. The signal is of the form $\exp(-t/T_2^*)\cos(-\omega_0 t)$, where T_2^* is the experimental transverse relaxation time, including magnetic field inhomogeneities due to the apparatus as well as those intrinsic to the sample. Figure 17.15 shows the pulse sequence, the value of M_x, and the value of M_z. The signal is proportional to M_x. The pulses can be repeated after time T_R for signal averaging. It is necessary for T_R to be greater than $5T_1$ in order for M_z to return nearly to its equilibrium value between pulses.

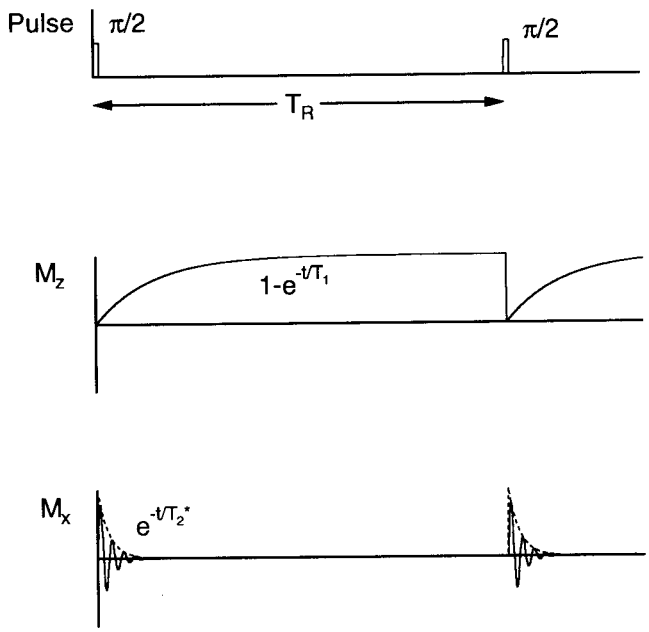

FIGURE 17.15. Pulse sequence and signal for a free induction-Decay measurement.

17.8.2. Inversion-Recovery (IR) Sequence

The inversion-recovery sequence allows measurement of T_1. A π pulse causes **M** to point along the $-z$ axis. There is not yet any signal at this point. M_z returns to equilibrium according to $M_z = M_0[1-2\exp(-t/T_1)]$. A $\pi/2$ interrogation pulse at time T_I rotates the instantaneous value of M_z into the xy plane, thereby giving a signal proportional to $M_0[1-2\exp(-T_I/T_1)]$, as shown in Fig. 17.16. The process can be repeated; again the repeat time must exceed $5T_1$.

You can see from Fig. 17.16 that there will be no signal at all if $T_I/T_1 = 0.693$. If T_I is less than this, the M_x signal will be inverted (negative). Unless special detector circuits are used which allow one to determine that M_x is negative, the results can be confusing.

Inversion recovery images take a long time to acquire and there is ambiguity in the sign of the signal. There are also problems with the use of a π pulse for slice selection [defined in Sec. 17.9; the details of the problems are found in Joseph and Axel (1984)].

17.8.3. Spin–Echo (SE) Sequence

The pulse sequence shown in Fig. 17.17 can be used to determine T_2 rather than T_2^*. Initially a $\pi/2$ pulse nutates **M** about the x' axis so that all spins lie along the rotating y' axis. Figure 17.17(a) shows two such spins. Spin a continues to precess at the same frequency as the rotating coordinate system; spin b is subject to a slightly smaller magnetic field and precesses at a slightly lower frequency, so that at time $T_E/2$ it has moved clockwise in the rotating frame by angle θ, as shown in Fig. 17.17(b). At this time a π pulse is applied that rotates all spins around the x' axis.

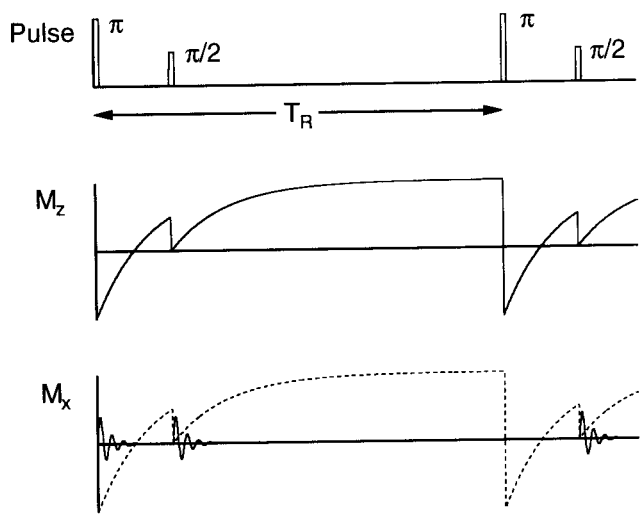

FIGURE 17.16. The inversion recovery sequence allows determination of T_1 by making successive measurements at various values of the interrogation time T_I.

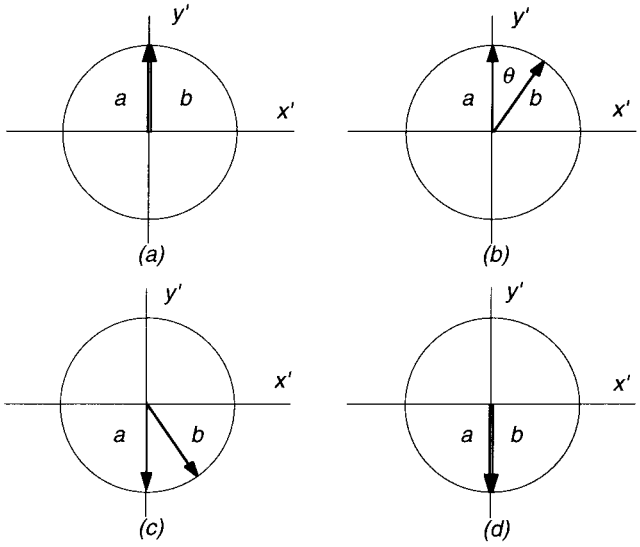

FIGURE 17.17. Two magnetic moments are shown in the $x'y'$ plane in the rotating coordinate system. Moment **a** rotates at the Larmor frequency and remains aligned along the y' axis. Moment **b** rotates clockwise with respect to moment **a**. (a) Both moments are initially in phase. (b) After time $T_E/2$ moment **b** is clockwise from moment **a**. (c) A π pulse nutates both moments about the x' axis. (d) At time T_E both moments are in phase again.

Spin a then points along the $-y'$ axis; spin b rotates to the angle shown in Fig. 17.17(c). If spin b still experiences the larger magnetic field, it continues to precess clockwise in the rotating frame. At time T_E both spins are in phase again, pointing along $-y'$ as shown in Fig. 17.17(d). This argument depends only on the fact that the magnetic field at the nucleus remained the same before and after the π pulse; it does not depend on the specific value of the dephasing angle. Therefore all of the spin dephasing that has been caused by a time-independent magnetic field is reversed in this process. There remains only the dephasing caused by fluctuating magnetic fields. Figure 17.18 shows the pulse sequence and signal.

17.8.4. Carr–Purcell (CP) Sequence

When a sequence of π pulses that nutate **M** about the x' axis are applied at $T_E/2$, $3T_E/2$, $5T_E/2$, etc., a sequence of echoes are formed, the amplitudes of which decay with relaxation time T_2. This is shown in Fig. 17.19. Referring to Fig. 17.17, one can see that the echoes are aligned alternately along the $-y'$ and $+y'$ axes. One advantage of the Carr–Purcell sequence is that it allows one to determine rapidly many points on the decay curve. Another advantage relates to diffusion. The molecules that contain the excited nuclei may diffuse. If the external magnetic field B_0 is not uniform, the molecules can diffuse to another region where the magnetic field is slightly different. As a result the

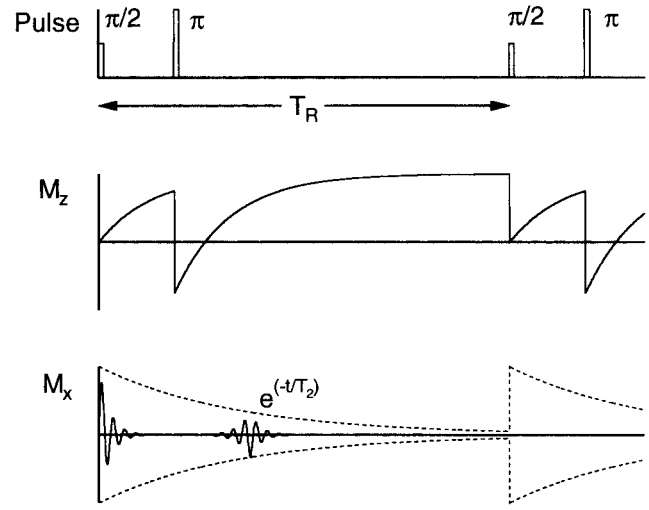

FIGURE 17.18. The pulse sequence and magnetization components for a spin–echo sequence.

rephasing after a π pulse does not completely cancel the initial dephasing. This effect is reduced by the Carr–Purcell sequence (see Problem 17.23).

17.8.5. Carr–Purcell–Meiboom–Gill (CPMG) Sequence

One disadvantage of the CP sequence is that the π pulse must be very accurate or a cumulative error builds up in successive pulses. The Carr–Purcell–Meiboom–Gill sequence overcomes this problem. The initial $\pi/2$ pulse nutates **M** about the x' axis as before, but the subsequent

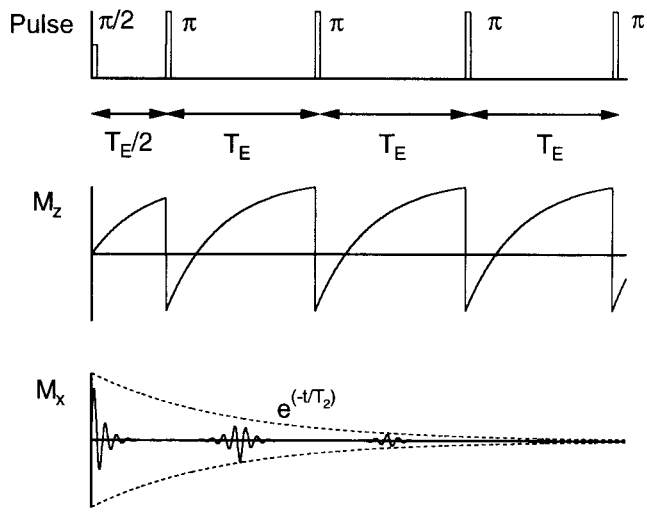

FIGURE 17.19. The Carr–Purcell pulse sequence. All pulses nutate about the x' axis. Echoes alternate sign. The envelope of echoes decays as $\exp(-t/T_2)$, where T_2 is the unrecoverable transverse relaxation time.

π pulses are shifted a quarter cycle in time and rotate about the y' axis. This is shown in Figs. 17.20 and 17.21.

17.9. IMAGING

There are many more techniques available for imaging with magnetic resonance than there are for computer tomography (CT). They are reviewed by Joseph (1985) and by Cho, Jones, and Singh (1993). An excellent new book that discusses pulse sequences in great detail along with signal-to-noise ratio and aspects of coil and electronics engineering has been written by scientists at Phillips Medical Systems [Vlaardingerbroek and den Boer (1996)].

We discuss two reconstruction methods here: projection reconstruction, which is similar to CT reconstruction, and a two-dimensional Fourier technique known as *spin warp* or *phase encoding*, which forms the basis of the techniques actually used in most machines. Our discussion is based on a spin–echo pulse sequence, repeated with a repetition time T_R as shown in Fig. 17.18.

17.9.1. Slice Selection

Suppose we were to apply a $\pi/2$ pulse in a 1.5-T machine ($\omega_0 = 401\times10^6$ s^{-1}; $f_0 = 63.9$ MHz). If the duration of this pulse is to be 5 ms, it will require a constant amplitude of the radiofrequency magnetic field

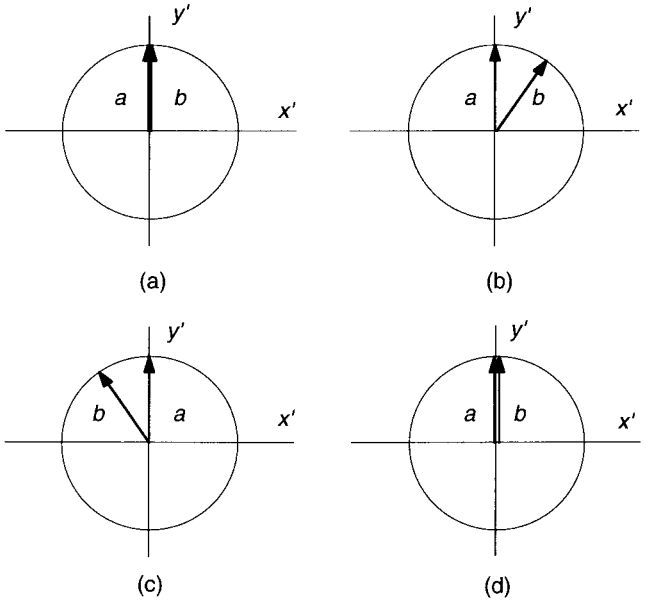

FIGURE 17.20. The effect of the Carr–Purcell–Meiboom–Gill pulse sequence on the magnetization. This is similar to Fig. 17.17 except that the π pulses rotate around the y' axis. Moment **b** rotates clockwise in the $x'y'$ plane. (a) Both moments are initially in phase. (b) After time $T_E/2$ moment **b** is clockwise from moment **a.** (c) A π pulse rotates both moments about the y' axis. (d) At time T_E both moments are in phase again.

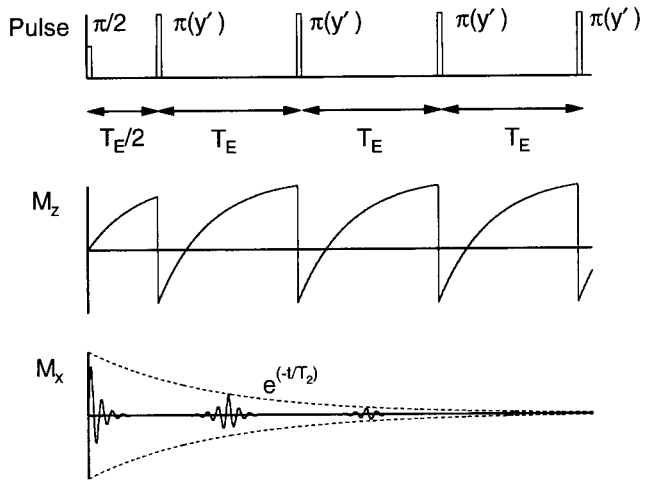

FIGURE 17.21. The CPMG pulse sequence.

$$B_1 = \pi/\gamma\Delta t = 2.35\times10^{-6}\ \text{T}. \qquad (17.38)$$

The pulse lasts for 3×10^5 cycles at the Larmor frequency. The frequency spread of the pulse is about 200 Hz. This would excite all the proton spins in the sample.

For MR imaging, we want to select a thin slice in the sample. In order to select a thin slice (say $\Delta z = 1$ cm) we apply a *magnetic field gradient* in the z direction while applying a specially shaped B_1 signal. In a static magnetic field B_0, the field lines are parallel. The field strength is proportional to the number of lines per unit area and does not change. With the gradient applied in the volume of interest, the field lines converge, and the field increases linearly with z as shown in Figs. 17.22(a) and 17.22(b):

$$B_z(z) = B_0 + G_z z. \qquad (17.39)$$

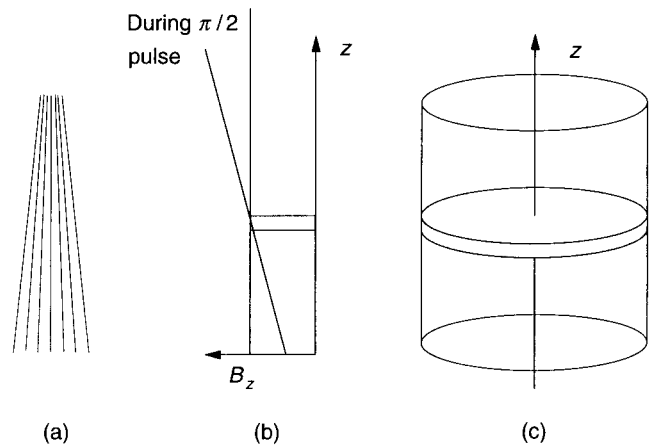

FIGURE 17.22. (a) Magnetic field lines for a magnetic field that increases in the z direction. (b) A plot of B_z vs z with and without a gradient. (c) After application of a field gradient in the z direction during the specially shaped rf pulse, all of the spins in the shaded slice are excited, that is, they are precessing in the xy plane.

We adopt a notation in which G represents a partial derivative of the z component of the magnetic field:

$$G_x \equiv \partial B_z/\partial x,$$
$$G_y \equiv \partial B_z/\partial y, \qquad (17.40)$$
$$G_z \equiv \partial B_z/\partial z.$$

In a typical machine, $G_z = 5\times10^{-3}$ T m^{-1}. For a slice thickness $\Delta z = 0.01$ m, the Larmor frequency across the slice varies from $\omega_0 - \Delta\omega$ to $\omega_0 + \Delta\omega$, where $\Delta\omega = \gamma G_z \Delta z/2 = 6.68\times10^3$ s^{-1} ($\Delta f = 1.064$ kHz).

It is possible to make the signal $B_x(t)$ consist of a uniform distribution of frequencies between $\omega_0 - \Delta\omega$ and $\omega_0 + \Delta\omega$, so that all protons are excited in a slice of thickness $\pm\Delta z/2$. Let the amplitude of B_x in the interval $(\omega, d\omega)$ be A. Using Eq. (11.55), $B_x(t)$ is given by

$$B_x(t) = \frac{A}{2\pi}\int_{\omega_0-\Delta\omega}^{\omega_0+\Delta\omega}\cos(\omega t)\,d\omega$$
$$= \frac{A\Delta\omega}{\pi}\frac{\sin(\Delta\omega t)}{\Delta\omega t}\cos(\omega_0 t). \qquad (17.41)$$

This has the form $B_1(t)\cos(\omega_0 t)$, where $B_1(t) = (A\Delta\omega/\pi)\sin(\Delta\omega t)/(\Delta\omega t)$. The function $\sin(x)/x$ has its maximum value of 1 at $x = 0$. It is also called the $\mathrm{sinc}(x)$ function. The angle ϕ through which the spins are nutated is

$$\phi = \int_{-\infty}^{\infty}\omega_1(t)\,dt = \frac{\gamma}{2}\int_{-\infty}^{\infty}B_1(t)\,dt$$
$$= \frac{\gamma A\Delta\omega}{2\pi}\int_{-\infty}^{\infty}\frac{\sin(\Delta\omega t)}{\Delta\omega t}\,dt$$
$$= \frac{\gamma A}{2}.$$

For a $\pi/2$ pulse, $A = \pi/\gamma$. The maximum value of B_1 is therefore $\Delta\omega/\gamma = G_z\Delta z/2$, as shown in Fig. 17.23. The B_x pulse does not have an abrupt beginning; it grows and decays as shown. In practice, it is truncated at some distance from the peak where the lobes are small.

While the gradient is applied, the transverse components of spins at different values of z precess at different rates. Therefore it is necessary to apply a gradient G_z of opposite sign after the $\pi/2$ pulse is finished in order to bring the spins back to the phase they had at the peak of the slice selection signal. When the gradient is removed all of the spins in the slice shown in Fig. 17.22(a) precess at the Larmor frequency in the xy plane.

17.9.2. Readout in the *x* Direction

The voltage induced in the pickup coil surrounding the sample is proportional to the free induction decay of **M** in the entire slice. That is, the voltage signal induced in the pickup coil is proportional to $\int M(x,y,z)\cos(-\omega_0 t)f(t)dV$,

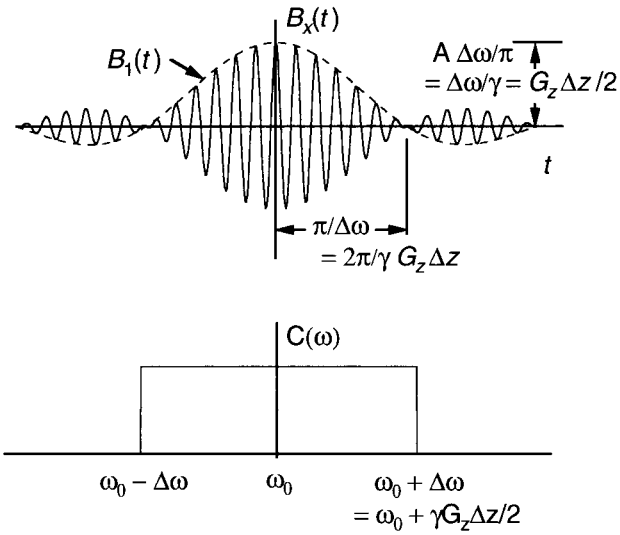

FIGURE 17.23. (a) The $B_x(t)$ signal shown is used to selectively excite a slice. It consists of $\cos(\omega_0 t)$ modulated by a "sinc(x)" or $\sin(x)/x$ pulse $B_1(t)$. (b) The frequency spectrum contains a uniform distribution of frequencies.

where $M(x,y,z)$ is the magnetization per unit volume that was nutated into the xy plane, $\cos(-\omega_0 t)$ represents the change in signal as **M** rotates in the xy plane at the Larmor frequency, and $f(t)$ represents relaxation, signal buildup during an echo, and so on. The initial free-induction-decay signal is ignored. Figure 17.24 shows the echo after a subsequent π pulse.

We assume that changes in $f(t)$ are slow compared to the Larmor frequency and neglect them here. Then the signal from an element $dx\,dy$ in the slice is

$$v(t) = A\,dx\,dy\Delta z\,M(x,y,z)\cos(-\omega_0 t). \qquad (17.42)$$

Constant A includes all the details of the detecting coils and receiver.

Suppose that B_z is given a gradient G_x in the x direction during the echo signal ("during readout"), as shown in Fig.

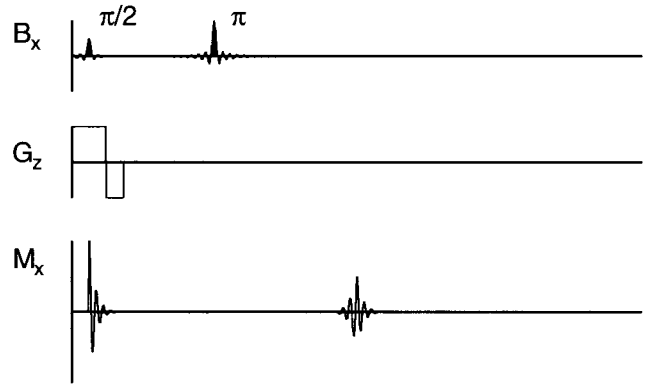

FIGURE 17.24. A slice selection pulse sequence. A $\pi/2$ B_x (rf) pulse while a gradient G_z is applied nutates the spins in a slice of thickness Δz into the xy plane. A negative G_z gradient restores the phase of the precessing spins. The echo after the π pulse is from the entire slice.

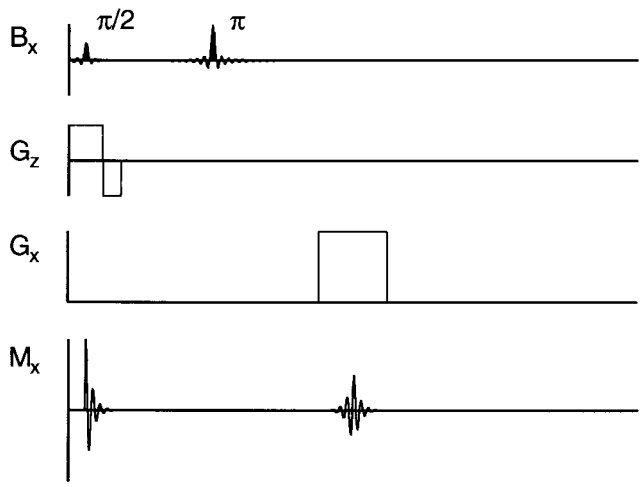

FIGURE 17.25. The pulse sequence for x readout. After slice selection, a gradient G_x is applied during readout. The echo signal between ω and $\omega+d\omega$ is proportional to the magnetization in a strip between x and $x+dx$, integrated over all values of y.

17.25. The spins that echo in the shaded slice between x and $x+dx$ in Fig. 17.26 will be precessing with a Larmor frequency between ω and $\omega+d\omega$, where $\omega=\omega_0+\gamma G_x x$. The signal from the entire slice is

$$v(t)=A\Delta z\int dx\left(\int dy\ M(x,y,z)\right)\cos[-\omega(x)t]. \tag{17.43}$$

We use the fact that $\omega(x)=\omega_0+\gamma G_x x$ to write the signal as

$$v(t)=A\Delta z\int dx\left(\int dy\ M(x,y,z)\right)\cos(\omega_0 t+\gamma G_x x t). \tag{17.44}$$

Since the z slice has already been selected, let us simplify the notation by dropping the z dependence of M. The electronics in the detector multiply $v(t)$ by $\cos(\omega_0 t)$ or $\sin(\omega_0 t)$ and average over many cycles at the Larmor frequency. The results are two signals that form the basis for constructing the image:

$$s_c(t)=\overline{v(t)\cos(\omega_0 t)}\propto\int\int dx\ dy\ M(x,y)\cos(\gamma G_x x t),$$

$$s_s(t)=\overline{v(t)\sin(\omega_0 t)}\propto\int\int dx dy M(x,y)\sin(\gamma G_x x t). \tag{17.45}$$

The time average is over many cycles at the Larmor frequency but a time short compared to $2\pi/\gamma G_x x_{\max}$.

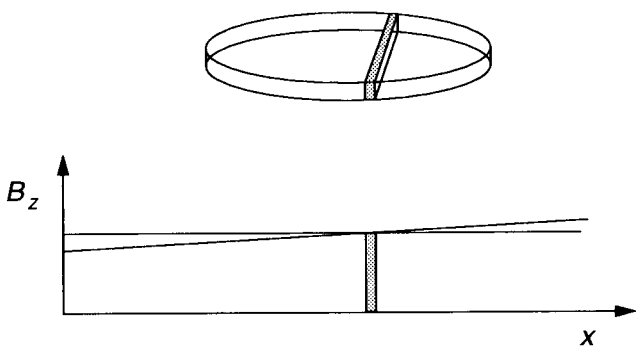

FIGURE 17.26. Because the gradient G_x is applied during readout, the Larmor frequency of all spins in the shaded slice is between ω and $\omega+d\omega$.

17.9.2.1. Projection Reconstruction

By inspection of Eq. (17.45) and remembering the relationship between ω and x, we see that the Fourier transforms of $s_c(t)$ and $s_s(t)$ are both proportional to $\int dy\ M(x,y)$. (Of course, the signals are digitized and one actually deals with discrete transforms.) This means that s_c or s_s can be Fourier analyzed to determine the amount of signal in the frequency interval $(\omega,d\omega)$ corresponding to (x,dx), which is proportional to the projection $\int M(x,y)\ dy$ along the shaded strip. In Sec. 12.8 we learned how to reconstruct an image from a set of projections. The entire readout process can be therefore be repeated with the gradient rotated slightly in the xy plane (that is, with a combination of G_x and G_y during readout). This is indicated in Fig. 17.27, which indicates many scans, with different values of G_x and G_y, related by

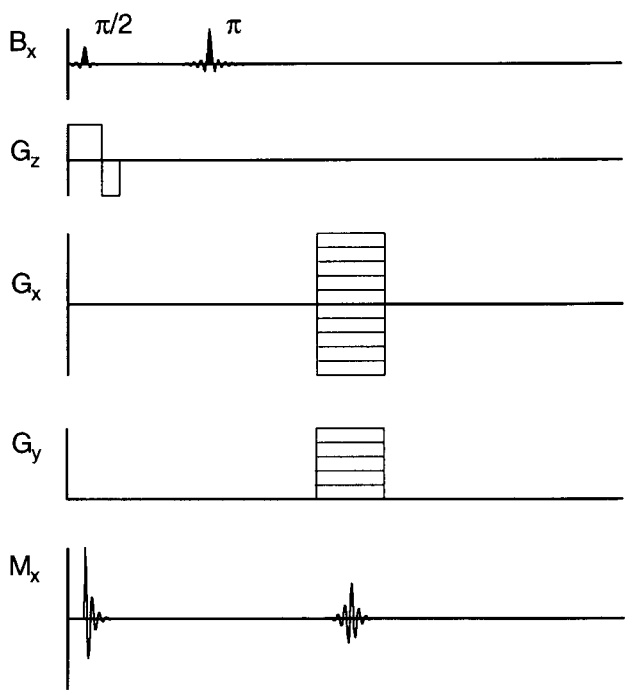

FIGURE 17.27. Projection reconstruction techniques can be used to form an image. A series of measurements are taken, each with simultaneous gradients G_x and G_y.

$G_x/G_y=\tan\theta$, where θ is the angle between the projection and the x axis. All of the techniques for reconstruction from projections that were developed for computed tomography can be used to reconstruct $M(x,y)$. Sending the proper combination of currents through the x and y gradient coils rotates the gradient; no rotating mechanical components are needed.

17.9.2.2. Phase Encoding

Techniques are available for magnetic resonance imaging that are not available for computed tomography. They are based on determining directly the Fourier coefficients in two or three dimensions. The basic technique is called *spin warp* or *phase encoding*.

We wish to construct an image of $M(x,y)$, modified by the function $f(t)$ that accounts for relaxation, etc. For simplicity of notation we again assume f is unity and suppress the z dependence, since slice selection has already been done. We will construct $M(x,y)$ from its Fourier transform. The Fourier transform of $M(x,y)$ is given by Eqs. (12.9):

$$M(x,y)=\left(\frac{1}{2\pi}\right)^2\int_{-\infty}^{\infty}dk_x\int_{-\infty}^{\infty}dk_y[C(k_x,k_y)\cos(k_xx+k_yy)+S(k_x,k_y)\sin(k_xx+k_yy)]. \tag{17.46a}$$

with the coefficients given by

$$C(k_x,k_y)=\int_{-\infty}^{\infty}dx\int_{-\infty}^{\infty}dy\ M(x,y)\cos(k_xx+k_yy), \tag{17.46b}$$

$$S(k_x,k_y)=\int_{-\infty}^{\infty}dx\int_{-\infty}^{\infty}dy\ M(x,y)\sin(k_xx+k_yy). \tag{17.46c}$$

Our problem is to determine C and S and from them construct the image.

The information from the x readout gives us $C(k_x,0)$ and $S(k_x,0)$ directly. We show this for the cosine transform. From Eq. (17.46b)

$$C(k_x,0)=\int dx\left(\int dyM(x,y)\right)\cos(k_xx). \tag{17.47}$$

Comparing this to the expression for $s_c(t)$ in Eq. (17.45), we see that

$$C(k_x,0)\propto s_c(k_x/\gamma G_x). \tag{17.48a}$$

Similarly,

$$S(k_x,0)\propto s_s(k_x/\gamma G_x). \tag{17.48b}$$

The times at which s_c and s_s are measured and therefore the values of k_x are, of course, discrete. The discussion in Sec. 12.6 shows that the values of k_x are multiples of the lowest spatial frequency:

$$k_x=m\ \Delta k=2\pi m/D.$$

The corresponding times to measure the signal are

$$t_m=\frac{2\pi m}{D\gamma G_x}.$$

The spatial extent of the image or "field of view" D determines the spacing Δk_x. The desired pixel size determines the maximum value of k_x or m:

$$\Delta x=\frac{\pi}{k_{\max}}=\frac{D}{2m_{\max}}.$$

The discrete values of k_x are shown in Fig. 17.28(a).

The next problem is to make a similar determination for nonzero values of k_y. To do so, a gradient of B_z in the y direction is applied at some time between slice selection and readout. This makes the Larmor frequency vary in the y direction. If the phase-encoding pulse is due to a uniform gradient that lasts for a time T_p, the total phase change is

$$\Delta\phi=\int\omega(t)\ dt=\gamma G_yT_py=k_yy. \tag{17.49}$$

The readout signal, Eq. (17.43), is replaced by

$$v(t)=A\ \Delta z\int dx\int dy\ M(x,y)\cos[-\omega(x)t+k_yy]. \tag{17.50}$$

Note that the added phase does not depend on t. However, the cosine term must now be included in both the x and y integrals. Carrying through the mathematics of the detection process shows that temporal Fourier transformation of the signals determines $C(k_x,k_y)$ and $S(k_x,k_y)$ for all values of k_x and for the particular of k_y determined by the phase selection pulse. Different values of the y gradient pulse give the coefficients for different values of k_y, as shown in Fig. 17.28. Both positive and negative gradients are used to give both positive and negative values of k_y. Application of a gradient G_x during the phase-encoding time (in addition to the readout gradient) changes the starting value of k_x. This allows one to determine the coefficients for negative values of k_x. This figure has been drawn without taking into account that the application of a π pulse changes k_x to $-k_x$ and k_y to $-k_y$. The gradients and signals for this spin–echo determination are shown in Fig. 17.29. The coefficients are substituted in Eq. (17.46a) to reconstruct $M(x,y,z)$ for the z slice in question.

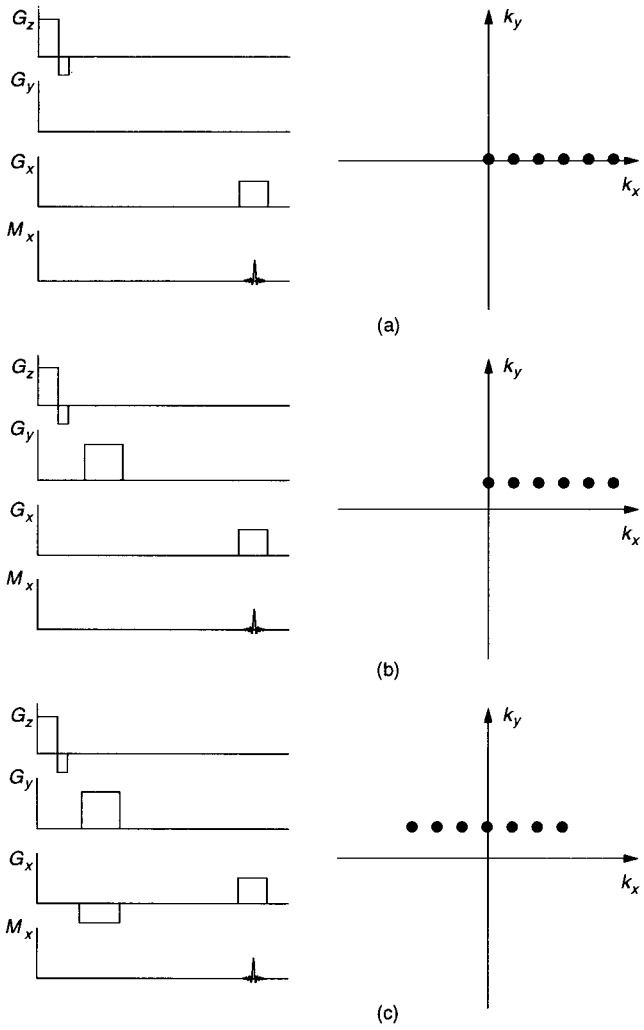

FIGURE 17.28. (a) The signal measured while the x gradient is applied gives the spatial Fourier transform of the image along the k_x axis. (b) The addition of a phase-encoding gradient sets a nonzero value for k_y so that the readout determines the spatial Fourier transform along a line parallel to the k_x axis. (c) Phase encoding along the x axis as well shifts the line along which the coefficients are determined.

17.9.3. Image Contrast and the Pulse Parameters

The appearance of an MR image can be changed drastically by adjusting the repetition time and the echo time. Problem 17.22 derives a general expression for the amplitude of the echo signal when a series of $\pi/2$ pulses are repeated every T_R seconds. The magnetic moment in the sample at the time of the measurement, considering both longitudinal and transverse relaxation, is

$$M(T_R,T_E)=M_0(1-2e^{-T_R/T_1+T_E/2T_1}+e^{-T_R/T_1})e^{-T_E/T_2}. \quad (17.51)$$

If $T_R \gg T_E$, this simplifies to

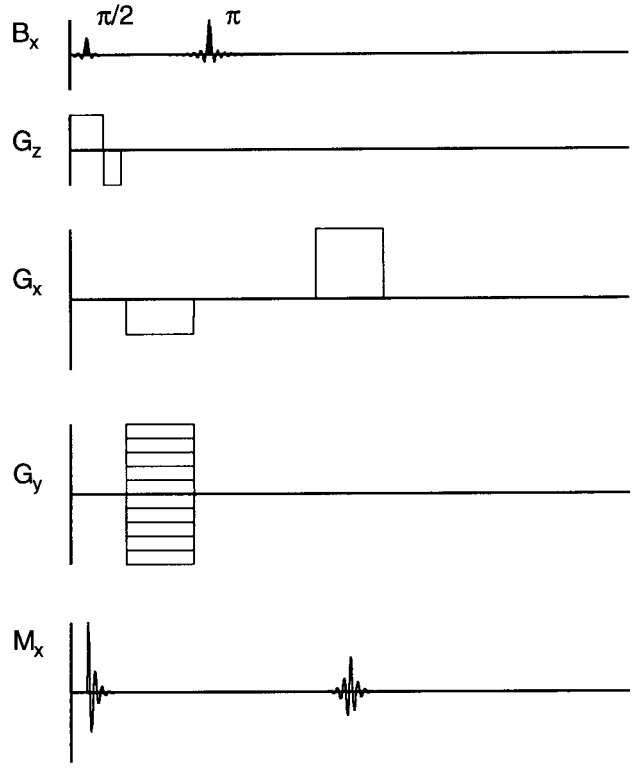

FIGURE 17.29. The signals in a standard phase encoding. The pulse sequence is repeated for each value of k_y.

$$M(T_R,T_E)=M_0(1-e^{-T_R/T_1})e^{-T_E/T_2}, \quad (17.52)$$

where M_0 is proportional to the number of proton spins per unit volume N, as shown in Eq. (17.10). We consider an example that compares muscle ($M_0=1.02$, $T_1=500$ ms, and $T_2=35$ ms) with fat ($M_0=1.24$, $T_1=200$ ms, and $T_2=60$ ms).

Figure 17.30 shows two examples where T_R is relatively long and M_0 returns nearly to its initial value between pulses. If the echo time is short, then the image is nearly independent of both T_1 and T_2 and it is called a *density-weighted image*. If T_E is longer, then the transverse decay term dominates and it is called a *T_2-weighted image*. The signal is often weak and therefore noisy because there has been so much decay.

Figure 17.31 shows what happens if the repetition time is made small compared to T_1. This is a *T_1-weighted image* because the differences in T_1 are responsible for most of the difference in signal intensity. Notice also that the very first pulse nutates the full M_0 into the transverse plane, so an echo after the first pulse would give an anomalous reading. Echoes are measured only for the second and later pulses. Suppose that the value of T_2 for fat had been shorter than the value for muscle. Then there would have been a value of T_E for which the two transverse magnetization curves crossed, and the two tissues would have been indistinguishable in the image. At larger values of T_E, their relative brightnesses would have been reversed. Figure 17.32 shows

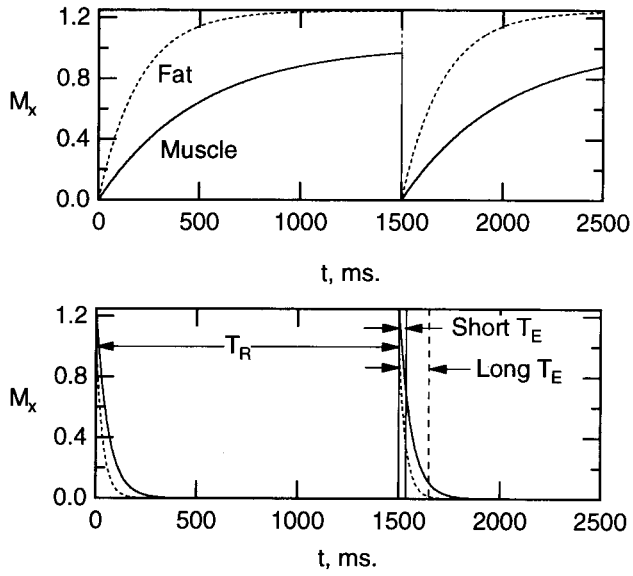

FIGURE 17.30. The intensity of the signal from different tissues depends on the relationship between the repetition time and echo times of the pulse sequence, and the relaxation times of the tissues being imaged. This figure and the next show the magnetization curves for two tissues: muscle (relative proton density 1.02, $T_1 = 500$ ms, $T_2 = 35$ ms) and fat (relative proton density 1.24, $T_1 = 200$ ms, $T_2 = 60$ ms). The repetition time is 1500 ms, which is long compared to the longitudinal relaxation times. A long echo time gives an image density that is very sensitive to T_2 values. A short echo time (even shorter than shown) gives an image that depends primarily on the spin density.

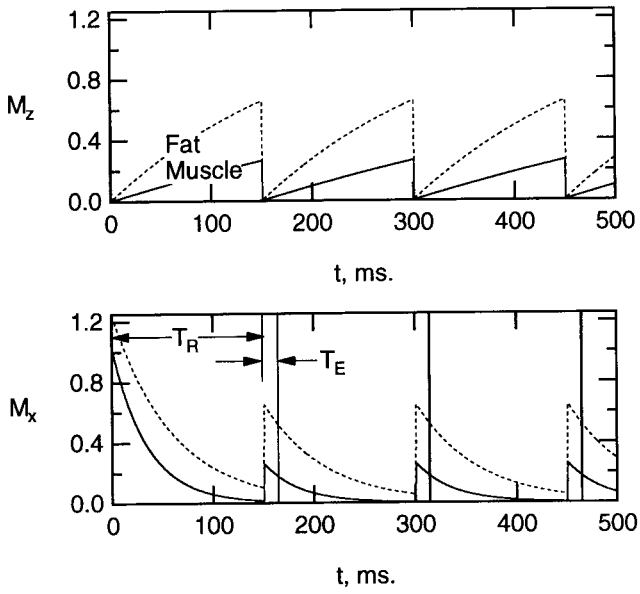

FIGURE 17.31. The tissue parameters are the same as in Fig. 17.30. The repetition time is short compared to the longitudinal relaxation time. As a result, the first echo must be ignored. With a short T_E, the image density depends strongly on the value of T_1.

FIGURE 17.32. Spin–echo images taken with short and long values of T_E, showing the difference in T_2 values for different parts of the brain. Photograph courtesy of R. Morin, Ph.D., Department of Diagnostic Radiology, University of Minnesota.

spin–echo images taken with two different values of T_E, for which the relative brightnesses are quite different.

17.9.4. Other Pulse Sequences

There are a large number of other pulse sequences in use, all of which are based on the fundamentals presented here. We mention only a few.

One of the problems with conventional spin echo is that one must wait a time T_R between measurements for different values of k_y. One way to speed things up is to use the intervening time to make measurement in a slice at a different value of z.

Fast spin echo or *turbo spin echo* uses a single $\pi/2$ pulse, followed by a series of π pulses, as shown in Fig. 17.33. Each π pulse produces an echo, though the echo amplitudes decay and a correction for this must be made in the image reconstruction. Each G_y pulse increments or "winds" the phase by a fixed amount. A negative G_x pulse resets the positions of the k_x values. Faster image acquisition sequences not only save time, but they may allow the image to be obtained while the patient's breath is held, thereby eliminating motion artifacts.

A variation on this is *echo planar imaging* (EPI) which eliminates the π pulses. It requires a magnet with a very uniform magnetic field, so T_2 (in the absence of a gradient) is only slightly greater than T_2^*. A small constant G_y is applied, and G_x oscillates as shown in Fig. 17.34. One of several applications is interlaced EPI. The $\pi/2$ pulse is synchronized with the heart beat. Data for several k_y values spread across the entire range of k space are acquired during the first beat, with additional sets of interleaved values acquired during subsequent beats (Fig. 17.35).

Other fast sequences only partially flip the spins into the xy plane.

A 3-dimensional Fourier transform of the image can be obtained by selecting the entire sample and then phase encoding in both the y and z directions while doing frequency readout along x. One must step through all

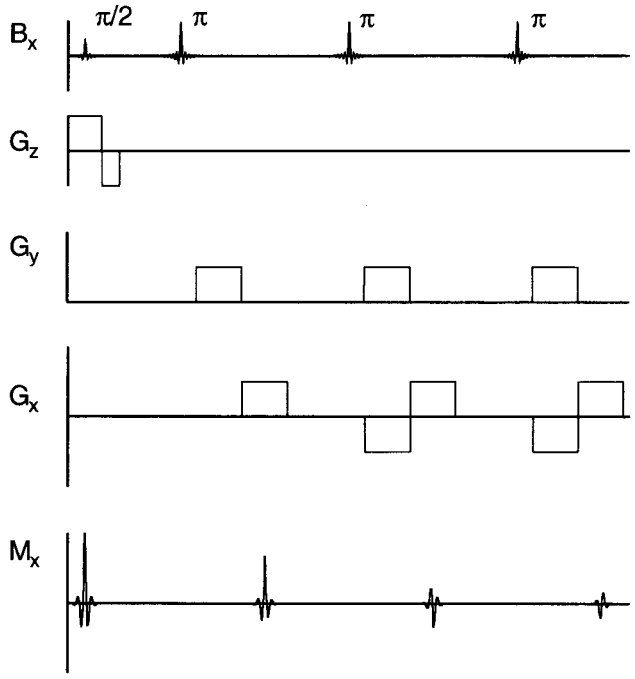

FIGURE 17.33. A fast spin echo sequence uses a single $\pi/2$ slice selection pulse followed by multiple echo rephasing pulses. A correction must be made for the transverse decay.

values of k_y for each value of k_z. This forms the basis for imaging very small samples with very high resolution (MRI microscopy).

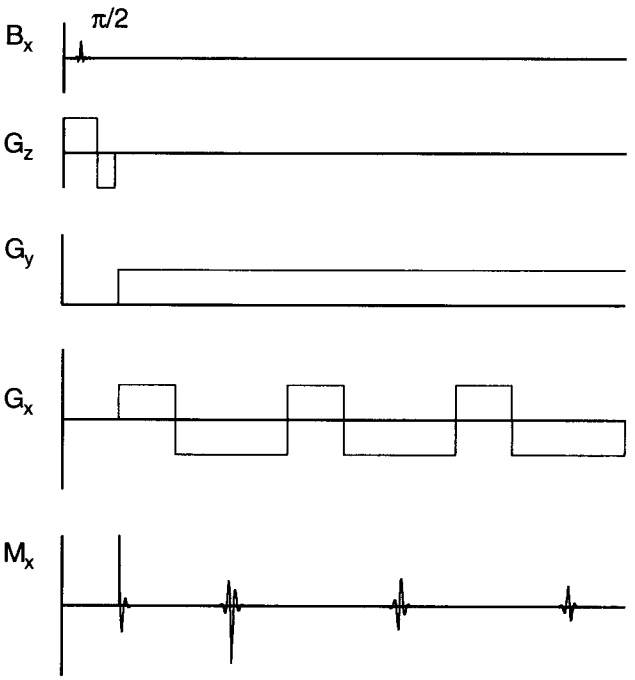

FIGURE 17.34. Echo planar imaging uses a very uniform magnet and eliminates the π rephasing pulses.

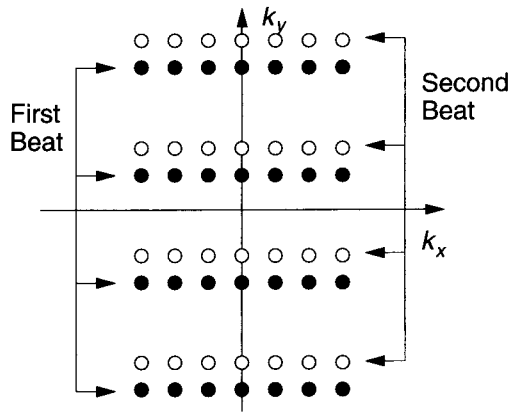

FIGURE 17.35. The excitation pulse for echo planar imaging (EPI) of the heart can be triggered by the electrocardiogram. Several values of k_y are sampled during the beat. Widely separated values of k_y are sampled on the first beat, with interleaved values on subsequent beats.

High spatial frequencies give the sharp edge detail in an image; the lowest spatial frequencies give the overall contrast. (We saw this in Figs. 12.16 and 12.17.) Changing the order of sampling points in k space can be useful. For example, when the image may be distorted by blood flow (see the Sec. 17.11), it is possible to change the gradients in such a way that the values of k near zero are measured right after the excitation. This gives the proper signal within the volume of the vessel. The higher spatial frequencies, which show vessel edges, are less sensitive to blood flow and are acquired later. Some acquisition sequences vary G_x and G_y as a function of time in such a way that a spiral path through k space is followed.

17.10. CHEMICAL SHIFT

If the external magnetic field is very homogeneous, it is possible to detect a shift of the Larmor frequency due to a reduction of the magnetic field at the nucleus because of diamagnetic shielding by the surrounding electron cloud. The modified Larmor frequency can be written as

$$\omega = \gamma B_0(1-\sigma). \tag{17.53}$$

Typical values of σ are in the range 10^{-5}–10^{-6}. They are independent of B_0, as expected for a diamagnetic effect proportional to B_0. Measurements are made by Fourier transformation of the free-induction-decay signal, averaged over many repetitions if necessary to provide the resolution required to detect the shift.

A great deal of work has been done with ^{31}P, because of its presence in adenosine triphosphate and adenosine diphosphate (ATP and ADP). Free energy is supplied for many processes in the body by the conversion of ATP to ADP. Figure 17.36 shows shifts in the ^{31}P peaks due to

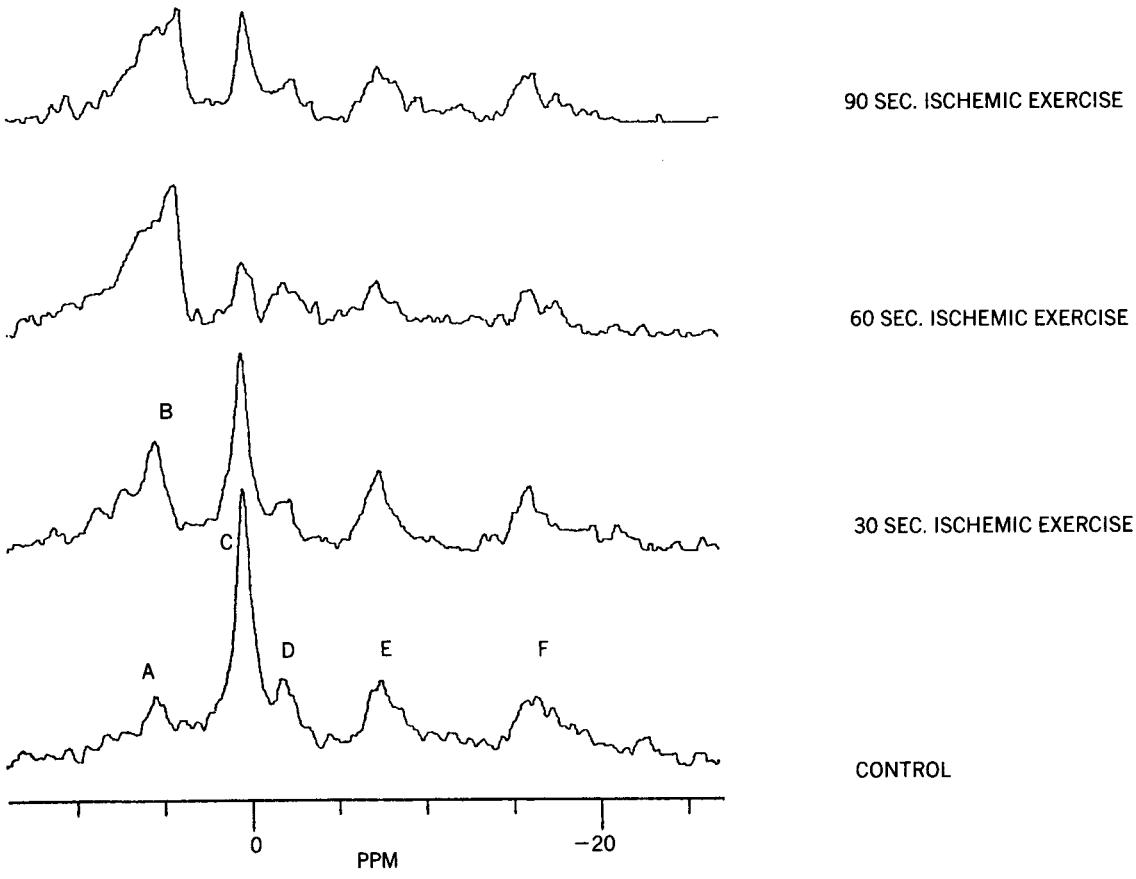

FIGURE 17.36. A series of ^{31}P NMR spectra from the forearm of a normal adult showing the change in various chemical-shift peaks with exercise. Peak A is inorganic phosphate; C is phosphocreatine; D, E, and F are from the three phosphates in ATP. One can see the disappearance of ATP and phosphocreatine with exercise, accompanied by the buildup of inorganic phosphate. From R. L. Nunally (1985). NMR spectroscopy for in vivo determination of metabolism; an overview, in S. R. Thomas and R. L. Dixon, eds. *NMR in Medicine: The Instrumentation and Clinical Applications*, College Park, MD, AAPM. Used by permission.

metabolic changes. With exercise the ATP and phosphocreatine peaks diminish and the inorganic phosphate peak increases.

It is also possible to make chemical shift images. An FID signal is measured for each volume element. Slice selection followed by phase encoding in two dimensions can be used (Fig. 17.37), or phase encoding can be used in all three directions. Because of the number of measurements required, spatial resolution is usually limited to 32×32 or 64×64. Figure 17.38 shows an ^{31}P image of the brain.

Metabolites containing hydrogen can also be measured, but special efforts are required to eliminate artefacts (distortions) due to the very strong signals from water and lipids [Hu *et al.* (1995)].

17.11. FLOW EFFECTS

Flow effects can distort a magnetic resonance image. Spins initially prepared with one value of **M** can flow out of a slice before the echo and be replaced by spins that had a different initial value of **M**. This is called *washout*. Spins that have been shifted in phase by a field gradient can flow to another location before the readout pulse is applied. Axel (1985) reviews the effect on images. This technique has also been used to measure blood flow [Battocletti *et al.* (1981)].

To understand the washout effect consider a simple model in which a blood vessel is perpendicular to the slice, as shown in Fig. 17.39. To simplify further, assume that all the blood flows with the same speed v, independent of where it is in the vessel. This is called *plug flow*.

First consider washout of the excited spins. Suppose that at time $T_E/2$ a π pulse is applied to the slice in Fig. 17.39 and that the echo is measured at time T_E. The shaded area in the vessel represents new blood that flows in during time t. If the flow velocity is zero, no new blood flows in, all of the blood in the slice was excited, and the signal has full strength. If the velocity is greater than $2\Delta z/T_E$, all of the spins that were flipped by the pulse will leave the sensitive region by the time of the echo, and there will be no signal.

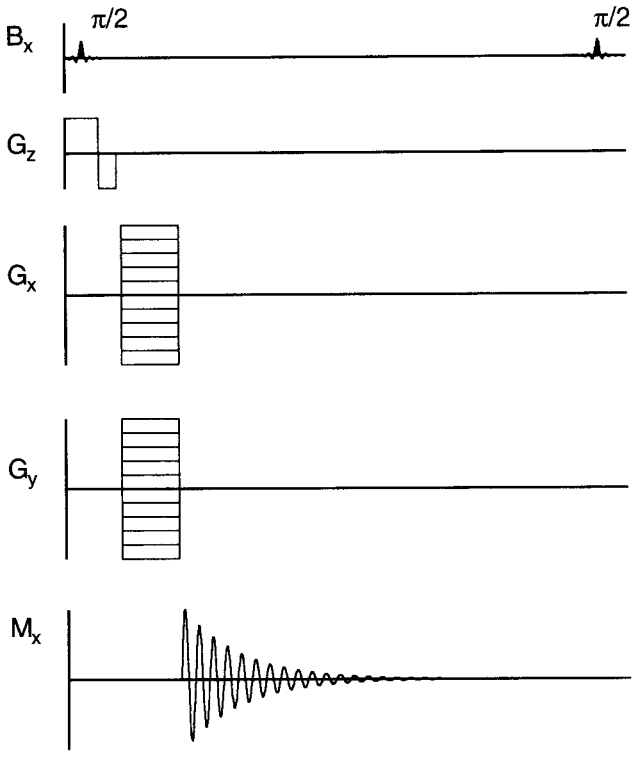

FIGURE 17.37. A possible pulse sequence to measure free induction decay (FID). Slice selection is used in the z direction, and phase encoding is applied in both the x and y directions before the FID signal is measured.

Because we assume plug flow, the fraction washed out is a linear function of velocity up to the critical value of v. The fraction of excited spins remaining at T_E is given by

$$f=\begin{cases} 1-\dfrac{vT_E}{2\Delta z}, & v<2\Delta z/T_E \\ 0, & v\geqslant 2\Delta z/T_E \end{cases}. \tag{17.54}$$

Now consider washout of spins between pulses. We saw that the effect of repetition and echo times on the MRI signal is given by Eq. (17.51), which, if $T_R \gg T_E$, simplifies to Eq. (17.52). For low velocities ($v<\Delta z/T_R$) there is an enhancement of the signal because blood with a larger value of M_z flows into the sensitive region. For $vT_R<\Delta z$, the factor in parentheses in Eq. (17.52) is replaced by

$$\frac{vT_R}{\Delta z}+\left(1-\frac{vT_R}{\Delta z}\right)(1-e^{-T_R/T_1}).$$

The first term represents spins that flow in and the second those that still remain and that are still affected by the previous pulse. This can be rearranged as

$$(1-e^{-T_R/T_1})+\frac{vT_R}{\Delta z}\,e^{-T_R/T_1}. \tag{17.55}$$

This factor has the value $1-\exp(-T_R/T_1)$ for small v and is replaced by unity for $v>\Delta z/T_R$. In this simple model, the effect on the signal is the product of Eqs. (17.54) and (17.55).

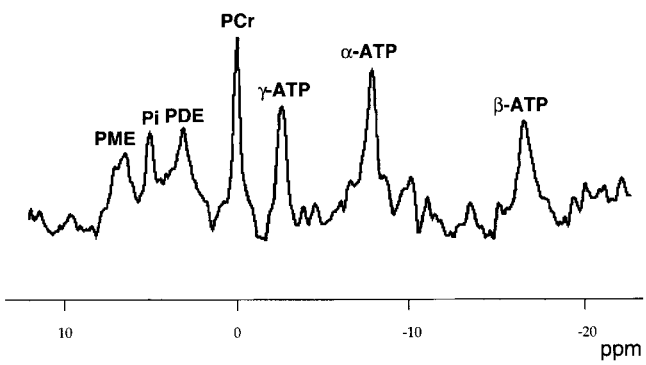

(a)

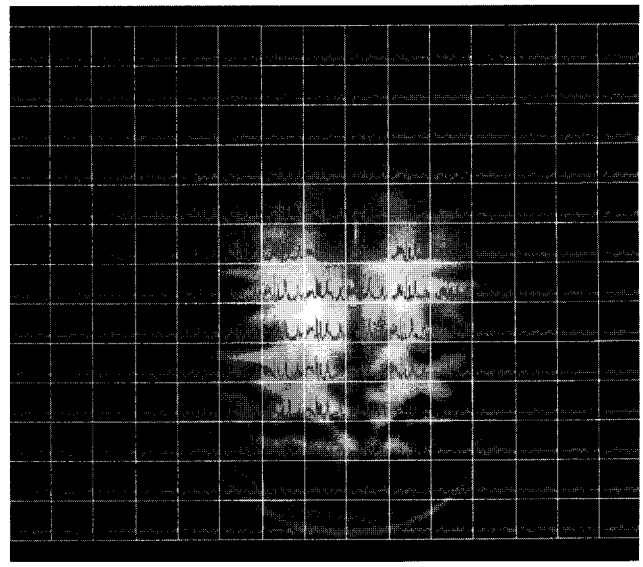

(b)

FIGURE 17.38. A ^{31}P chemical shift image obtained by making a Fourier transform of the FID signal to determine the various chemical peaks. (a) The chemical shift spectrum in a single volume element. (b) A map of the chemical shift image between +10 and −20 ppm. From X. Hu, W. Chen, M. Patel, and K. Ugurbil (1995). Chemical shift imaging: An introduction to its theory and practice. Chap. 65.4 in J. D. Bronzino, ed. *The Biomedical Engineering Handbook*.

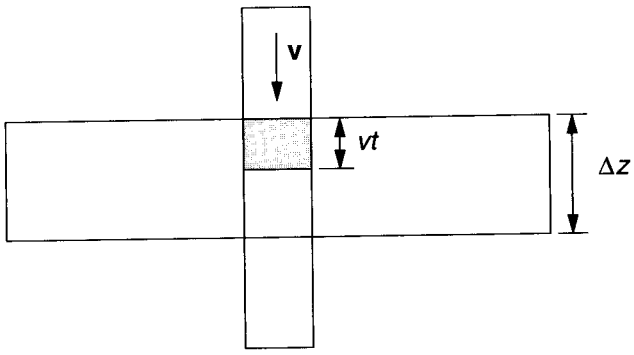

FIGURE 17.39. A blood vessel is perpendicular to the slice. The model developed in the text assumes plug flow, that is, all of the blood is flowing with the same speed v.

More complicated models can be developed, and phase changes because the blood flows through magnetic field gradients are also important.

SYMBOLS USED IN CHAPTER 17

Symbol	Use	Units	First used on page
a	Loop radius	m	502
a,b	Arbitrary constants	$J\,T^{-1}\,m^{-2}$	498
f	Fraction		513
$\hbar$	Planck's constant (reduced)	J s	494
i	Current	A	493
k_B	Boltzmann factor	$J\,K^{-1}$	494
k_x,k_y,k_z	Spatial frequency	m^{-1}	508
m	Mass	kg	493
m	Azimuthal quantum number		494
q	Electric charge	C	493
r	Radius	m	493
t	Time	s	493
v	Velocity	$m\,s^{-1}$	493
v	Voltage difference	V	502
x	Dimensionless variable		506
x',y',z'	Rotating axes	m	496
x,y,z	Axes	m	494
Δz	Slice thickness	m	506
B,**B**	Magnetic field	T	492
C	Constant in expression for relaxation time	s^2	501
$C(k),S(k)$	Fourier transforms	$T\,m^{-2}$	508
E	Energy	J	499
G_xG_y,G_z	Gradient of B_z in the x, y, or z direction	$T\,m^{-1}$	506
I	Nuclear angular momentum	$kg\,m^2\,s^{-1}$	494
I	Nuclear angular momentum quantum number		494
K	Constant		501
L	Orbital angular momentum	$kg\,m^2\,s^{-1}$	493
M,**M**	Magnetization	$J\,T^{-1}\,m^{-3}$	494
N	Number of spins per unit volume	m^{-3}	494
S	Area	m^2	493
S	Spin angular momentum	$kg\,m^2\,s^{-1}$	494
S	Spin angular momentum quantum number		494
T	Temperature	K	494
T_E	Time of echo	s	503
T_I	Interrogation time	s	503
T_R	Repetition time between $\pi/2$ pulses	s	503
T_1	Longitudinal relaxation time	s	495
T_2	Transverse relaxation time	s	495
T_2^*	Experimental transverse relaxation time	s	501
U	Potential energy	J	493
V	Volume	m^3	502
α	Arbitrary angle		498
γ	Gyromagnetic ratio	$T^{-1}\,s^{-1}$	493
μ,$\boldsymbol{\mu}$	Magnetic moment	$J\,T^{-1}$	492
μ_0		$T\,m\,A^{-1}$	499
θ	Angle		493
σ	Chemical shift factor		511
τ,$\boldsymbol{\tau}$	Torque	N m	492
τ	Shift time for autocorrelation	s	500
τ_C	Correlation time	s	500
ω_1	Angular frequency for B_1 rotation	s^{-1}	498
ω	Angular frequency	s^{-1}	494
ω_0	Larmor angular frequency	s^{-1}	495
ϕ	Azimuthal angle		499
ϕ	Phase		508
Φ	Magnetic flux	weber ($T\,m^2$)	502
$\boldsymbol{\Omega}$	Angular velocity vector	s^{-1}	497

PROBLEMS

Section 17.1

17.1. Show that for a particle of mass m located at position $\mathbf{r}$ with respect to the origin, the torque about the origin is the rate of change of the angular momentum about the origin.

Section 17.2

17.2. Show that the units of γ are $T^{-1}\,s^{-1}$.

17.3. Find the ratio of the gyromagnetic ratio in Table 17.1 to the value $q/2m$ for the electron and proton.

Section 17.3

17.4. Evaluate the quantity $\gamma m\hbar B/k_BT$ and the Larmor frequency for electron spins and proton spins in a magnetic fields of 0.5 and 4.0 T at body temperature (310 K).

17.5. Verify that $\Sigma 1 = 2I+1$, $\Sigma m = 0$, and $\Sigma m^2 = I(I+1)(2I+1)/3$, when the sums are taken from $-I$ to I, in the cases that $I = \frac{1}{2}$, 1, and $\frac{3}{2}$.

17.6. Obtain an expression for the magnetization analogous to Eq. (17.10) in the case $I = \frac{1}{2}$ when one cannot make the assumption $\gamma\hbar B/k_BT \ll 1$. (This is called the *Langevin equation.*)

17.7. Calculate the coefficient of B in Eq. (17.10) for a collection of hydrogen nuclei at 310 K when the number of hydrogen nuclei per unit volume is the same as in water.

Section 17.4

17.8. Verify that Eqs. (17.16) are a solution of Eqs. (17.15).

17.9. Calculate the value of $M_x^2+M_y^2+M_z^2$ for relaxation [Eqs. (17.16)] when $T_1 = T_2$.

17.10. Equations (17.16) correspond to a solution of the Bloch equations in the presence of a static field B. What would be the solutions if initially $M_x = 0$, $M_y = 0$, and $M_z = -M_0$?

Section 17.5

17.11. (a) Use Fig. 17.6 to derive Eq. (17.17). (b) Show that

$$M_{x'} = M_x \cos\theta + M_y \sin\theta,$$

$$M_{y'} = -M_x \sin\theta + M_y \cos\theta.$$

(c) Combine these equations with the equations for M_x and M_y to show that the application of both transformations brings one back to the starting point.

17.12. Calculate $M^2 = M_x^2+M_y^2+M_z^2$ for the solution of Eqs. (17.29) and compare it to the results of Problem 17.9.

Section 17.6

17.13. Use Eqs. (17.31) to find the magnetic field at one proton due to the other proton in a water molecule when both proton spins are parallel to each other and perpendicular to the line between the protons. The two protons form an angle of 104.5° and are each 96.5×10^{-12} m from the oxygen.

17.14. The magnetic field at a distance of 0.15 nm from a proton is 4×10^{-4} T. What change in Larmor frequency does this ΔB cause? How long will it take for a phase difference of π radians to occur between a precessing spin feeling this extra field and one that is not?

17.15. Consider a collection of spins that are aligned along the x axis at $t = 0$. They precess in the xy plane with different angular frequencies spread uniformly between $\omega - \Delta\omega/2$ and $\omega + \Delta\omega/2$. If the total magnetic moment per unit volume is M_0 at $t = 0$, show that at time $T = 4/\Delta\omega$ it is $M_0 \sin(2)/2 = 0.455M_0$.

17.16. What is the contribution to the transverse relaxation time for a magnetic field of 1.5 T with a uniformity of 1 part per million? The nonrecoverable relaxation time of brain is about 2.5 ms. What dominates the measured transverse relaxation in brain?

Section 17.7

17.17. In solving this problem, you will develop a simple model for estimating the radio-frequency energy absorption in a patient undergoing an MRI procedure.

(a) Consider a uniform conductor with electrical conductivity σ. If it is subject to a changing magnetic field $B_1(t) = B_1\cos(\omega_0 t)$, apply Eq. (8.18) to a circular path of radius R at right angles to the field to show that the electric field at radius R has amplitude $E_0 = R\omega_0 B_1/2$. (Because this is proportional to R, the model gives the skin dose, along the path for which R is largest.)

(b) Use Ohm's law in the form $j = \sigma E$ to show that the time average power dissipated per unit volume of material is $p = \sigma E_0^2/2 = \sigma R^2\omega_0^2 B_1^2/8$ and that if the mass density of the material is ρ, the specific absorbed rate (SAR) or dose rate is $\mathrm{SAR} = \sigma R^2\omega_0^2 B_1^2/8\rho$.

(c) If the radio-frequency signal is not continuous but is pulsed, show that this must be modified by the "duty cycle" factor $\Delta t/T_R$, where Δt is the pulse duration and T_R is the repetition period.

(d) Combine these results with the fact that rotation through an angle θ (usually π or $\pi/2$) in time Δt requires $B_1 = 2\theta/\gamma\,\Delta t$ and that $\omega_0 = \gamma B_0$, to obtain $\mathrm{SAR} = (1/T_R\Delta t)(\sigma/2\rho)(R^2/4)B_0^2\theta^2$.

(e) Use typical values for the human body—$R = 0.17$ m, $\sigma = 0.3$ S m^{-1}—to evaluate this expression for a $\pi/2$ pulse.

(f) For $B_0 = 0.5$ T and $\mathrm{SAR} < 0.4$ W kg^{-1} determine the minimum value of Δt for $T_R = 1$ s. Also find B_1.

(g) For 180 pulses, what is the dose in Gy? (This should not be compared to an x-ray dose because this is non-ionizing radiation.)

17.18. Use Eq. (17.37) to calculate the initial amplitude of a signal induced in a one-turn coil of radius 0.5 m for protons in an 1-mm cube of water at 310 K in a magnetic field of 1.0 T. (The answer will be too small a signal to be useful; multiple-turn coils must be used.)

Section 17.8

17.19. Plot the maximum amplitude of an inversion recovery signal vs the interrogation time if the detector is sensitive to the sign of the signal and if it is not.

17.20. (a) Obtain an analytic expression for the maximum value of the first and second echo amplitudes in a Carr–Purcell pulse sequence in terms of T_2 and T_E. (b) Repeat for a CPMG pulse sequence.

17.21. Consider the behavior of M_z in Figs. 17.19 and 17.21. The general equation for M_z is $M_z = M_0 + Ae^{-t/T_1}$. After several π pulses, the value of M_z is flipping from $-b$ to b. Find the value of b.

17.22. Consider a spin–echo pulse sequence (Fig. 17.18). Find

(a) M_z just before the π pulse at $T_E/2$,

(b) M_z just after the π pulse at $T_E/2$,

(c) M_z just before the $\pi/2$ pulse at T_R, and

(d) the first and second echo amplitudes as a function of T_E, T_R, T_1 and T_2. (The second amplitude is the same as all subsequent amplitudes.)

17.23. This problem shows how to extend the Bloch equations to include the effect of diffusion of the molecules containing the nuclear spins in an inhomogeneous external magnetic field. Since **M** is the magnetization per unit volume, it depends on the total number of particles per unit volume with average spin components $\langle \mu_x \rangle$, $\langle \mu_y \rangle$, and $\langle \mu_z \rangle$. In the rotating coordinate system there is no precession. In the absence of relaxation effects $\langle \boldsymbol{\mu} \rangle$ does not change. In that case changes in **M** depend on changes in the concentration of particles with particular components of $\langle \boldsymbol{\mu} \rangle$, so the rate of change of each component of $\langle \boldsymbol{\mu} \rangle$ is given by a diffusion equation. For example, for $M_{x'}$,

$$\frac{\partial M_{x'}}{\partial t} = D\nabla^2 M_{x'}.$$

If the processes are linear this diffusion term can be added to the other terms in the Bloch equations. Suppose that there is a uniform gradient in B_z, G_z, and that the coordinate system rotates with the Larmor frequency for $z=0$. When z is not zero, the rotation term does not quite cancel the $(\mathbf{M}\times\mathbf{B})_z$ term.

(a) Show that the x and y Bloch equations become

$$\frac{\partial M_{x'}}{\partial t} = +\gamma G_z z M_{y'} - \frac{M_{x'}}{T_2} + D\nabla^2 M_{x'},$$

$$\frac{\partial M_{y'}}{\partial t} = -\gamma G_z z M_{x'} - \frac{M_{y'}}{T_2} + D\nabla^2 M_{y'}.$$

(b) Show that in the absence of diffusion

$$M_{x'} = M_x(0)e^{-t/T_2}\cos(\gamma G_{zz} z t),$$

$$M_{y'} = M_y(0)e^{-t/T_2}\sin(\gamma G_{zz} z t).$$

(c) Suppose that **M** is uniform in all directions. At $t=0$ all spins are aligned. Spins that have been rotating faster in the plane at $z+\Delta z$ will diffuse into plane z. Equal numbers of slower spins will diffuse in from plane $z-\Delta z$. Show that this means that the phase of **M** will not change but the amplitude will.

(d) It is reasonable to assume that the amplitude of the diffusion-induced decay will not depend on z as long as we are far from boundaries. Therefore try a solution of the form

$$M_{x'} = M_x(0)e^{-t/T_2}\cos(\gamma G_z z t)A(t),$$

$$M_{y'} = M_y(0)e^{-t/T_2}\sin(\gamma G_z z t)A(t),$$

and show that A must obey the differential equation

$$\frac{1}{A}\frac{dA}{dt} = -D\gamma^2 G_z^2 t^2,$$

which has a solution $A(t) = \exp(-D\gamma^2 G_z^2 t^3/3)$.

(e) Show that if there is a rotation about y' at time $T_E/2$, then at time T_E M_x is given by

$$M_x(T_E) = -M_0\exp(-T_E/T_2)\exp(-D\gamma^2 G_z^2 T_E^3/12).$$

Hint: This can be done formally from the differential equations. However it is much easier to think physically about what each factor in the expressions shown in (d) for M_x and $M_{y'}$ mean. This result means that a CPMG sequence with short T_E intervals can reduce the effect of diffusion when there is an external gradient.

17.24. A commercial MRI machine is operated with a magnetic gradient of 3 mT m^{-1} while a slice is being selected. What is the effect of diffusion? Use the diffusion constant for self-diffusion in water and the results of Problem 17.23. Compare the correction factor to $\exp(-T_E/T_2)$ when $T_2 = 75$ ms.

Section 17.9

17.25. Show that an alternative expression for the field amplitude required for a $\pi/2$ pulse is $B_1 = B_0\pi/\omega_0\,\Delta t = B_0/2\nu\Delta t$.

17.26. A certain MRI machine has a static magnetic field of 1.0 T. Spins are excited by applying a field gradient of 3×10^{-3} T m^{-1}. If the slice is to be 5 mm thick, what is the Larmor frequency and the spread in frequencies that is required?

17.27. Consider a pair of gradient coils of radius a perpendicular to the z axis and located at $z = \pm\sqrt{3}a/2$. The current flows in the opposite direction in each single-turn coil.

(a) Use the results of Problem 8.6 to obtain an expression for B_z along the z axis.

(b) For a gradient of 5×10^{-3} T m^{-1} at the origin and $a = 10$ cm, find the current required in a single-turn coil.

(c) Find the force on a coil in a field of 1.0 T.

17.28. Find a linear approximation for Eq. (17.52) for very small values of T_E and T_R, and discuss why it is called a T_1-weighted image.

17.29. How rapid is the transverse dephasing during a typical selection pulse if no compensating negative gradient is used?

17.30. Relate the resolution in the y direction to G_y and T_p.

17.31. Discuss the length of time required to obtain a 256×256 image in terms of T_R and T_E. The field of view is 15 cm square. Consider both projection reconstruction and spin warp images. Introduce any other parameters you need.

17.32. The limiting noise in a well-designed machine is due to thermal currents in the body. The noise is proportional to B_0 and the volume V_n sampled by the radio-frequency pickup coil. The noise is proportional to $T^{-1/2}$, where T is the time it takes to acquire the image. Show that the signal-to-noise ratio is proportional to $B_0 T^{1/2} V_v / V_n$, where V_v is the volume of the picture element.

Section 17.11

17.33. Use the model of Sec. 17.11 to plot the flow correction as a function of velocity for $T_E = 10$ ms, $T_1 = 900$ ms, and $T_2 = 400$ ms, when (a) $T_R = 50$ ms, (b) $T_R = 200$ ms.

REFERENCES

Axel, L. (1985). Flow effects in magnetic resonance imaging, in S. R. Thomas and R. L. Dixon, eds. *NMR in Medicine: The Instrumentation and Clinical Applications*. College Park, MD, AAPM.

Battocletti, J. H., R. E. Halbach, and S. X. Salles-Cunha (1981). The NMR blood flow meter—Theory and history. *Med. Phys.* **8**: 435–443.

Cho, Z.-H., J. P. Jones, and M. Singh (1993). *Foundations of Medical Imaging*. New York, Wiley-Interscience.

Dixon, R. L., K. E. Ekstrand, and P. R. Moran (1985). The physics of proton NMR: Part II—The microscopic description. In S. R. Thomas and R. L. Dixon, eds. *NMR in Medicine: The Instrumentation and Clinical Applications*. College Park, MD, AAPM.

Hu, X, W. Chen, M. Patel, and K. Ugurbil (1995). Chemical shift imaging: An introduction to its theory and practice. Chap. 65.4 in J. D. Bronzino, ed. *The Biomedical Engineering Handbook*. Boca Raton, CRC.

Joseph, P. M. (1985). Pulse sequences for magnetic resonance imaging. In S. R. Thomas and R. L. Dixon, eds. *NMR in Medicine: The Instrumentation and Clinical Applications*. College Park, MD, AAPM.

Joseph, P. M., and L. Axel (1984). Potential problems with selective pulses in NMR imaging systems. *Med. Phys.* **11**(6): 772–777.

Nunally, R. L. (1985). NMR spectroscopy for in vivo determination of metabolism: An overview. In S. R. Thomas and R. L. Dixon, eds. *NMR in Medicine: The Instrumentation and Clinical Applications*. College Park, MD, AAPM.

Slichter, C. P. (1978). *Principles of Magnetic Resonance*. New York, Springer.

Thomas, S. R., and R. L. Dixon, eds. (1985). *NMR in Medicine: The Instrumentation and Clinical Applications*. College Park, MD, AAPM.

Vlaardingerbroek, M. T., and J. A. den Boer (1996). *Magnetic Resonance Imaging: Theory and Practice*. Berlin, Springer.